Kazakh National Research Technical University named after Satbayev K.I.

ӘОЖ: 615.47:616-072.7(43)   Manuscript
On the right

YESHMUKHAMETOV AZAMAT NURLANOVICH

Design and Development of Novel Wire-driven Continuum Robot Arm with Passive
Sliding Disc Mechanism: Kinematic Analyses and Experiments

6D071600 – Instrumentation Engineering

Dissertation to obtain the degree of Doctor of Philosophy (PhD)

Supervisor:
Candidate of technical science, associate professor
Seidakhmet Askar Zhunisovich

Foreign supervisor:
Doctor of Ph.D., professor
Yoshio Yamamoto

Republic of Kazakhstan
Almaty, 2020

Table of Contents

REGULATORY REFERENCES

References in accordance with the following standards are used in the dissertation:

MECT 6.38.90 – Identified documentation systems. System of organizational and decree documentation. Requirements for registration of documents.

MECT 7.32.2001 – System of standards for information, library and publishing. Research report. Structure and rules of design.

MECT 8.417 – 81 – The system of ensuring the integrity of state dimensions. Units of physical quantities

Definitions

1. *Continuum robot* – a robot with continuos structure and slender design with flexible backbone, such as octopus arm or elephant trunk.
2. *Wire-tension*- tithened cable with applied force or mass to the both sides of the wire.
3. *Backbone* –continuum robot center part for holding the whole structure.
4. *Hyper-redundant mechanism*- when robot mechanism has more degrees of freedom than used motors.
5. *Clearance effect*- when the detail or robot part has a gap or small space, such kind og gap might affect negatively.

Chapter I. INTRODUCTION

1.1.   Research background

Today, technology and the economy are growing dramatically, and such significant growth also brings many challenges. One of the challenges is a robot which could work in a confined and unstructured environment. Traditional rigid link robots cannot meet with these requirements. And to solve such a problem, many researchers proposed soft robots, hyper-redundant manipulators, and continuum robots. Because of flexible structures, however, continuum robots cannot manipulate weight and have a serious problem with accuracy. Based on conducted research on previous researchers and built robots, we came to the idea that among all continuous structured robots, wire-driven continuum manipulators have a great potential to be used widely in our daily life.

Recently, wire-driven mechanisms have been utilized in many biomechanical and medical robots because of the beneficial features of using wire. Firstly, since wires can transmit force from a distance, motorized joints are not required. Secondly, due to the flexibility of the wire, various designs for robots are possible. These features encourage engineers and scientists to develop more robots and devices using wires [1].

The backbone design of continuum robots can be divided into three main groups: discrete continuum robot, hard continuum robot, and soft continuum robot (Fig. 1-1). A discrete continuum robot arm backbone consists of universal joints and mostly actuates by cable. Moreover, a discrete continuum robot arm is relatively heavier and could produce more torque than other types of continuum robots. In other words, a discrete continuum arm looks like a multi-jointed robot arm or gripper [2]. Secondly, hard continuum robots represent robots using shape memory alloy and a spring backbone connected by spacer discs made of plastic or metal. A soft continuum robot arm backbone is made of rubber or silicone. Hard continuum robot and soft continuum robot features are similar. For instance, in their application, those robots are designed mostly for inspection purposes, such as minimally invasive surgery [3,4]. One of the main differences, though, is that because of its backbone type, the discrete continuum robot arm possesses greater torque and has a larger payload capacity. Relatively, discrete continuum robots provide higher payload capacity than other continuum manipulators [5,6].

In continuum manipulators, a wire-driven actuation system demonstrates great application potential due to its flexibility, dexterity, reachability, and safety for humans as well. Compared with other continuum robots using pneumatic and dielectric elastomer actuation systems, wire-driven manipulators provide high payload capacity and accuracy. However, wire-driven mechanisms have a problem with tension when the robot bends. Tension control for tendon mechanisms is still a challenging issue, and it demands additional equipment to compensate for slack during work (see Fig. 1-1).
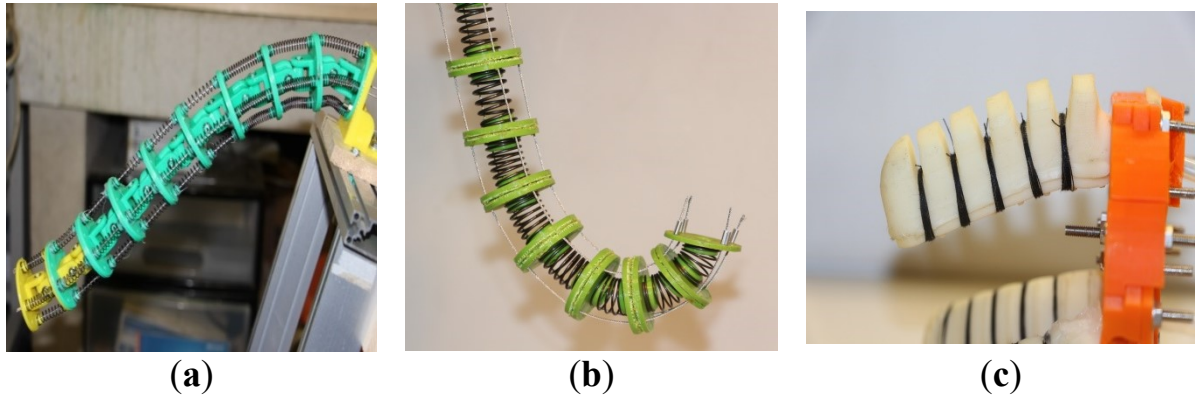
Fig. 1-1. Continuum robot backbone types. (**a**) Discrete hyper-redundant; (**b**) Hard continuum manipulator [6]; (**c**) Soft manipulator.

1.2. Related research works

Historically, the first continuum robot, named Tensor Arm, was designed in 1967 by Anderson and Horn [7]. The prototype's intended application was underwater manipulation; however, due to the limitation of the computing environment, the prototype could not be manipulated underwater [8]. In the 1990s, many efforts were made in continuum robots hardware design that modified the tendon-driven concept of Anderson/Horn and Hirose [9–12] (Table 1-1), and a new innovative backbone pneumatically actuated was created by Robinson and Davies [13]. Moreover, the size of the continuum manipulators was minimized for minimally invasive surgery, such as the HARP robot. HARP is a concentric tube manipulator. By inserting and rotating inner tubes with outer tubes, the robot can change its shape and bend into the desired position. However, the main drawback of this robot is its slow speed and lack of payload capacity [14]. Similarly, Zheng Li and his team developed a novel continuum robot arm for minimally invasive surgery named the constrained tendon-driven serpentine manipulator (CTSM). The rigidity of CTSM can be tuned in two ways: by controlling the tendon and by controlling the length of the bending section. As a result, continuum manipulators revolutionized minimally invasive surgery [15]. Furthermore, continuum robots became softer and more compliant. Ning Tang and his team developed a soft actuator driven by flexible shafts. The robot is fabricated using an FDM-based 3D printer that can print soft and flexible robot parts [4].

In recent works, Kang and his team first proposed an interlaced continuum robot, devised to follow the leader. However, in spite of its novelty, the robot structure is complicated, and the robot has poor payload capacity. [16]. Furthermore, Daekeun et al. proposed a wire-driven manipulator with constrained spherical joints for minimally invasive surgery. The proposed robot can reach a specified curvature, and it has low torsional stress as well. The main benefit of the robot design is a hole along the whole backbone, which provides space for additional medical tools [17]. Kai Xu also proposed a surgical robot with redundant backbones and constrained bending curvature for continuously variable stiffness. Additionally, Xu developed a unique actuation system for continuum manipulators, which prevents it from buckling under the pressure [18].

In terms of the wire-driven mechanism tension, there were many proposed solutions by scholars and engineers to compensate for the tension problem in wire-driven continuum robots. For example, Hyunki In and his team introduced a passive brake mechanism called a capstan brake. It operates as a one-way clutch and rotates in the winding direction. The proposed mechanism prevents the wire from escaping from the pulleys and compensates for tension [1]. Similarly, Kazuo Haiya proposed nonlinear springs to control wire tension. This method adjusts wire tension by utilizing the stiffness of the adjustable tendon, which is a light, cheap, and simple rubber material. The material expands and shrinks to adjust the tension on the cables [2]. Furthermore, Jung-Wook Suh proposed pulleyless rolling joints for wire-driven mechanisms. In his research, he utilized a diamond-shaped pulley for driving and joints. According to the results of his experiments, this kind of pulley prevented cables from slackening [3].

In terms of kinematic formulation of continuum manipulators, Webster and Jones made a great contribution to the formulation of both multi-section and concentric tube robots [5]. Zheng Li also proposed a similar method. He modified Walker's kinematic formulation for multi-section manipulators and relations using cable length variation [18]. Kinematics based on cable length variation was also proposed by X. Dong on twin-pivot continuum robot arm for gas turbine inspection [19]. Furthermore, this research proposed a kinematic formulation combined with kinetic force & torque equilibrium for an actual discrete cable-driven manipulators.

Table 1-1: History and classification of the continuum robot arm.

Literature	Continuous/ discrete	Actuation	Application
Tensor arm (Anderson and Horn, 1967)	D	Tendon	Underwater manipulation
OCRobotics (Buckingham, 2002, 2008)	D	Tendon	Reactor repair
Elephant Trunk (Hanna and Walker, 2003)	D	Tendon/spring	Bio-inspired manipulation
Elephant Trunk (Ciezlak and Morenki, 1999	C	Tendon/spring	Liquid transportation
EMMA (Bostelman et. All, 1997)	D	Tendon/spring	Sanding, Nuclear
Backbone (Gavagne et.all, 2003)	C	Tendon/Rod	General purpose
Artroscope (Dario et.all, 2000	D	Tendon/Rods	General purpose
Catheter (Camarilo et.all, 2008,2009	C	Tendon/sleeve	Cardiac surgery

Colobot (Chen et.all, 2004, 2005, 2006)	C	Pneumatic	Colonoscopy
OctArm (Jones and Walker, 2006a)	C	Pneumatic	General-purpose
Slim Slime1 (Ohno and Hirose, 2000, 2001)	C	Pneumatic	Search and rescue
Air-OCTOR (Jones and Walker, 2006)	C	Tendon/Pneumatic	General-purpose

According to the past continuum robot studies, the robot design optimization is still on going. The vast majority robots mentioned above still have several drawbacks. One of the main problem: the wire-tension problem has not yet been solved, which is the problem that continuum robots frequently suffer from slacking of their wires during motion, which consequently affects to the robot payload capacity. Moreover, control of continuum robots is also challenging issue, wire-driven mechanism requires actuators driving simultaneously to prevent any slack or derailing issues.

1.3. Related studies on continuum robot control

Attention to the continuum manipulators dramatically increased in the last couple of decades. One of the main reasons is a reaching ability in the unstructured and confined space, because of inherited flexible features of the backbone [20]. Therefore, continuum manipulator finds more application in rescue operations and minimally invasive surgery as well.

According to the continuum robot application, the vast majority continuum manipulators are being used in minimally invasive surgery, inspection and reactor repairement work. All of those applications are teleoperated, because of human assistance is highly required when robot intended workspase is an extremely constrained.

The actuating systems for the continuum robots are divided into three groups: wire-driven, fluid-driven (hydro or pneumo) actuation system, and dielectric elastomer system. The most popular actuation system is wire-driven because wire-driven actuation has a potential to provide more torque and also useful for maintenance. [21-24]. Also, pneumo actuators require more design space and maintenance difficulty. The latest actuation system is a polymer material called dielectric elastomer. This material can change the size by applying a voltage. Despite the material lightness, it requires high voltage, and the mechanical property of the material will degenerate after numerous applications.

Many researchers and engineers brought a valuable contribution to the development of continuum robots. In spite of their great dexterity features, controlling of continuum manipulator is still a seriously challenging issue. Because of intrinsic flexibility of the mechanism. continuum robots suffer from poor payload capacity which provides less accuracy in comparison with traditional rigid link manipulators [25-29].

Continuum manipulators, in comparison with conventional rigid link robots, have strong adaptability in constrained workspace [30]. Moreover, the continuous-bodied arm also can be utilized for grasping or enveloping objects with variable size and shape [31-33]. Therefore, robots with continuum manipulators are well suited for works such as inspection, harvesting, and rescue operations in a confined environment [34-35].

Continuum manipulators are mainly categorized into three types by their actuation system: tendon/wire/cable-driven continuum robots, robots based on a concentric tube, and fluid-driven continuum robots.

The main benefit of wire-driven manipulators resides in its high payload capacity due to high power transmitting in a low weight mobile body. Representative prototypes are "Elephant trunk" [36,37] and "Snake-arm" by OC Robotics [50].

Concentric tube-based continuum manipulators are also remotely actuated, and one of the main beneficial features is its potential of miniaturization [38-40].

Fluid-driven continuum manipulators (pneumatic or hydraulic) having a backbone can take a structure mimicking a human skeletal-muscular system [44].

Among mentioned above continuum manipulator types, wire-driven continuum robots represent a high applicable appliance for industrial or medical fields because of their high payload capacity and accuracy properties [41-43].

However, the main critical issue for wire-driven continuum manipulators resides in the difficulty of wire tension. Many researchers and engineers proposed several methods to prevent wire slack that frequently happens during operating. One of the most popular methods is to apply a conventional closed-loop PID control method. This method requires tension sensors equipped along all of the wire to feedback wire-tension to maintain an appropriate amount of tension [52-56]. Another method is adjusting wire tension by using motors with torque sensors. This method can maintain a certain wire tension level by the holding torque of the motor, [57-60]. These methods are premised on controlling one wire with one motor, which will incur a complicated simultaneous control of many motors if many wires drive the manipulator. In our previous research, we proposed to use an extensional spring along the wire [42], but such a method failed because of ineffectiveness and causes less precise motion of the robot.

Moreover, in terms of preventing wire slack, Phee et al. proposed a tendon-sheath method, where a wire is covered with sheath material to prevent wire derailing from pulleys [59]. Similarly, some researchers proposed to use a capstan brake that works unilaterally [60]. For single wire actuated robots such as in "Elephant trunk" [36,37] they proposed to utilize a winding drum to elongate and retract extra wires during the motion.

This research improved the previously developed passive pretension mechanism to solve wire slack and derailing problems [61]. The novelty of the proposed mechanism is its compact structure of controlling many wires-tensions in one place and to be used as sensors to provide wire-tension. The proposed device was developed to utilize on previously presented wire-driven discrete continuum robot arm named TakoBot [43].

1.4. Related studies on continuum robot application

Tomato is a high-demand fruit world wide, and the consumption is gradually increasing year by year. Manual harvesting of tomatoes is laborious, time-consuming, and inefficient, which makes it impractical in large-scale farms. Moreover, the tomato is very soft and prone to bruising, which makes harvesting and the grasping process difficult. Furthermore, one of the main problems in the agriculture sector is labour cost rising and labour shortages because agricultural work is not popular among young people [62]. Therefore, robotization of tomato harvesting could be one of the most efficient solutions to eliminate the problems mentioned above. However, many technological issues remain to be solved when considering robotization. This research proposes one approach for the robotization of tomato harvesting.

The main components in designing harvesting robots are a moving platform, a reaching manipulator, a grasping tool, and a tomato recognition algorithm. This research proposes a manipulating robot arm, a grasping tool, and a tomato recognition system.

Firstly, the most important component of the harvesting manipulator is the arm. Many researchers and engineers have proposed various types of robot arms for harvesting purposes. Many examples use a commercially available rigid link manipulator such as KUKA and Universal Robots [62-64,67]. Similarly, Wang et al. utilized a SCARA type serial manipulator mounted on the top of the mobile robot [65]. Takaaki proposed a hard continuum manipulator with a flexible structure, which has proven to be safe with wide reachability but possessing a low payload capacity [66]. Similar harvesting robot arms are proposed by Van et al. designed and developed a cucumber harvesting robot arm utilizing a thermal cutter, and its successful harvesting percentage was 74% [67]. Thus, the proposed continuum manipulator will contribute to improve the reachability to objects and manipulability of them, because actuated multi-section design and safety for the surrounded environment.

One of a challenging issues in fruit harvesting is the gripper design. The tomato is a fragile and soft fruit, so grasping the tomato should be gentle to avoid any bruising and smashing. Moreover, detaching the tomato is also challenging. For instance, Wang et al. developed a gripper with a clamp mechanism to cut the stem after grasping the tomato [65]. Similarly, Zhao et al. proposed a dual-arm SCARA robot, where one arm holds a tomato, and the second arm cuts the stem. This requires additional training for tomato stem detection, and the two arms should work synchronously with precision. Some researchers propose a vacuum machine with a sucking function and scissors [63]. Furthermore, Hiroaki et al. proposed a plucking gripper with an infinite rotational joint to automatically detach tomatoes [69], but the success rate of detaching in the real application was only 60%. A similar gripper design has also has been proposed by Root Ai Company and their Virgo robot having a SCARA type arm that detaches tomatoes by twisting them after grasping. [70]. Panasonic also presented a commercially available prototype tomato picker robot. The robot spends only 2-3 seconds per tomato, and now it is the fastest prototype [71]. However, the prototypes mentioned above cannot detach tomatoes from their

sepal, which may cause problems in terms of tomato durability during transportation. Thus, in our proposed prototype design, there are two semi-spherical cups with sharp blades on the edges to cut the stem at its sepal in a passive mechanical way.

For the harvesting work, a tomato recognition system is also a critical issue. There is much research on tomato recognition systems proposing some methods of discriminating mature tomatoes from non-mature tomatoes. One of the popular methods of tomato detection uses image data obtained by an RGB stereo camera [72-77]. Furthermore, the infrared method of tomato detection also could be used, which easily discriminate tomato color by using reflected light. [75-78]. In order to improve the tomato harvesting process, it employed machine learning based on a neural network to detect tomatoes and identify the ripeness of the tomato. This method could also be used for tomato classification, and it improves recognition accuracy [79-83].

This would present the robot applications in the agriculture sector for tomato harvesting purposes and a tomato detection system. As a manipulating arm, the previously presented discrete wire-driven continuum robot arm was used named as TakoBot [43]. Moreover, a special tomato gripper for grasping ripe tomatoes had been developed.

1.5. The purpose of the study

The purpose of the study is a development of wire-driven continuum robot arm with improved features on load capacity and manipulability. The survey of related research works on continuum manipulators elaborated above points out their advantages and drawbacks of continuum robots. The main drawback of continuum robot is its difficulty to sustain a certain level of backbone rigidity that leads to inaccuracy in motion and low load capacity. Moreover, the wire-driven mechanism proposed so far requires to drive all motors simultaneously to hold wire-tension and keep the structure stiff. Thus, based on numerous previously conducted experimental works, this research proposes a novel robot arm design and control methods. Furthermore, in this research, the robot kinetics & kinematics is also proposed in more physically reflected form than existing method of lumped kinematic system. This thesis shows the experimental and simulation results to certify the effectiveness of the proposed continuum robot. Finally, the thesis introduces an application of the proposed robot in an agricultural sector.

1.6. Organization of the thesis

The thesis is organized into 6 chapters; a brief outline of the thesis is as follows:

Chapter I. This chapter describes the research background and a brief survey of related research works. The chapter also described continuum robot types and classification.
Subsequently, it derives the research puposes and scopes.

Chapter II. This chapter describes the proposed robot design concept and design analysis. The purpose of the chapter is to give detailed information about robot design and components as well, such as continuum robot slender design, actuating unit design, and pretension mechanism design as well. Moreover, this chapter provides a design analysis of previously fabricated prototypes.

Chapter III. This chapter describes the proposed robot kinematic/kinetic formulations. Furthermore, kinematic analysis and motion case studies area provided as a validation of the proposed kinematics.

Chapter IV. This chapter deals with the robot control and control board schematics. It also describes types of control mode, which is used for controling the proposed robot as well as wire-tension feedback control method.

Chapter V. This chapter describes the robot application and experiments. The proposed robot finds its application in the agriculture sector because the slender flexible design makes continuum robot safety for the surrounded environment and reachable in the confined workspace. Moreover, for its application, a machine learning tool is used for tomato detection and recognition.
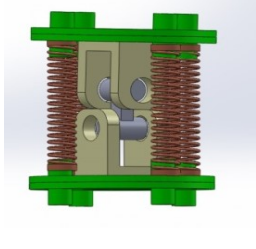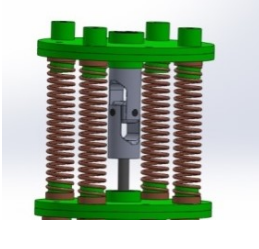
Chapter VI. This chapter is devoted to conclusive remarks with some scope of future works.

Chapter II. DESIGN CONCEPT

2.1. Design analysis

The backbone is a crucial part of continuum manipulators. Therefore, based on the backbone structure, robot characteristics, and capabilities may be different. One of the main reasons for using continuum manipulators is payload capacity and bending capability. For the best robot backbone design, two prototypes (with sliding discs and without sliding discs) had been manufactured (Table 2-1) and conducted several tests to figure out the optimal continuum robot design. In all prototypes, the same springs and motors were used.

Table 2-1. TakoBot prototypes comparison table

Features		
Name	Non-sliding	Sliding
Segment size	Length: 35mm Diameter: 50mm	Length 35mm Diameter: 50mm
Num. of segments	10	10
Max. bending angle	$< 45^0$	$< 45^0$-50^0
Torsional motion	no	yes
Required Torque	$\tau > 0.69$N•m	$\tau < 0.69$N•m
Max. payload capacity	175g	220g
Control	Difficult	Easy

2.2. Robot design overview

This research thesis developed a wire-driven discrete continuum robot arm named TakoBot (in Japanese Tako means octopus). Ian Walker had proposed a similar prototype in 1999 so-called "Elephant trunk" [27]. Universal joints interconnected the proposed robot actuated by wire and springs and spacer disc. Based on this design, we build our first prototype, but we faced a serious problem related to wire friction and wire slack, also driving of slack wire led to derailing of the cable from the pulleys. Moreover, such design required more torque, and the motor section was very big, which created a lot of problems. Furthermore, this

research will focus on identification of optimal distance for the continuum part segment length.
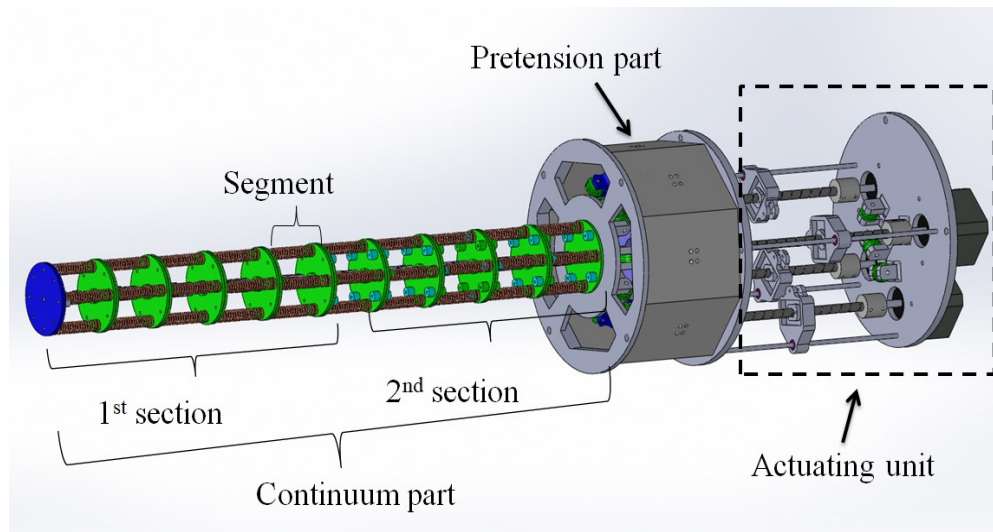

Fig. 2-1. CAD design of TakoBot

In the previous studies, wire-driven continuum manipulators had a problem with wire friction along the continuum part and bending curves. In the previous studies a prototype model does not show a pure bending, which means that wires occasionally inteferes with the robot parts and prevent a smooth rotation of joints.

In this research, a new type of continuum robot backbone so-called passive sliding disc mechanism was designed. This design is based on state of the art; natural animal samples such as octopus or elephant trunk, their trunk, or tentacles length are fixed, but the muscles can change the shape and arrangement depending on the grasping object. Thus, the proposed mechanism has a similar property, and the mechanism can distribute strain or bending stress in a smart way along the continuum part.4

2.3. Continuum structure design

The design of the proposed manipulator is demonstrated in Fig.2-1. This research would represent a modified version of the previous prototype with the non-sliding backbone disc (Fig. 2-3b). TakoBot with sliding discs consists of three parts: the continuum part, the pre-tension part, and the control box. The continuum part, the slender part of the robot, consists of two independent sections. Each section has five segments separated by discs that slide along a backbone shaft. The neighboring two rods are interconnected by a universal joint (Fig.2-2). Four compression springs are allocated at every 90 degrees between adjacent discs to transfer forces and are firmly fixed on the disc surface by spring pins. The discs, except for one that separates the first and second sections, slide along the backbone through the linear bearing equipped in the disc center.
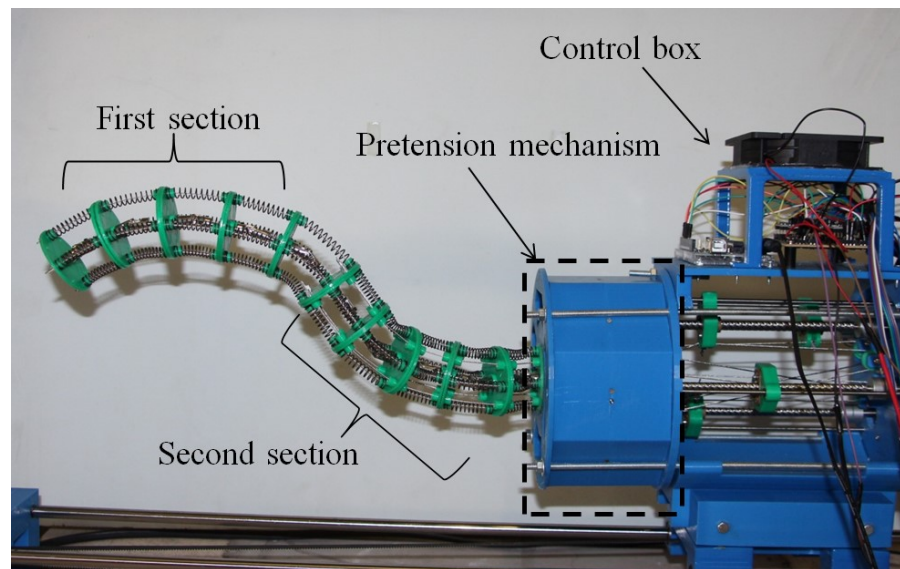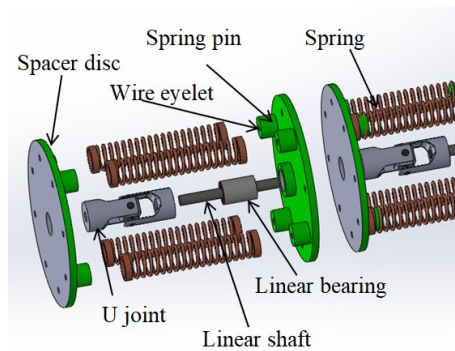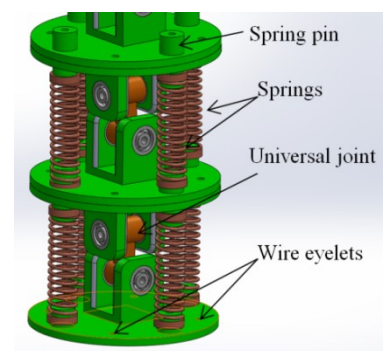
Fig. 2-2 TakoBot appearance.

Fig. 2-3 shows the sliding backbone disc design. The mechanism endows two degrees of freedom into every disc. One is a translational motion along the backbone axis, and the other is a rotational motion around the same axis.

(a) Sliding   (b) Non-sliding model

Fig.2-3 Single segment of sliding structure (a) and non-sliding model (b)

The previous non-sliding prototype was inspired by the Elephant Trunk robot (Walker and Hanna, 1999), where Walker used cable-routing spacer discs, universal joints, and extension springs [27].
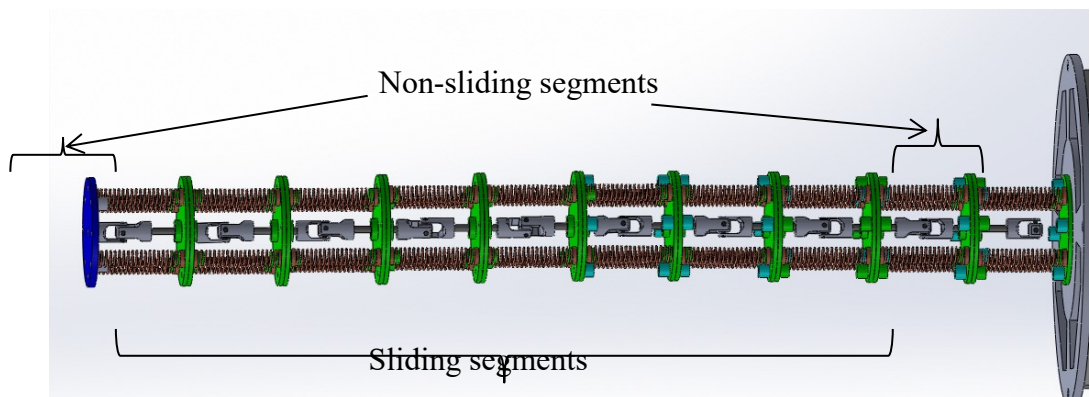
Fig.2-4 Slender part architecture of TakoBot
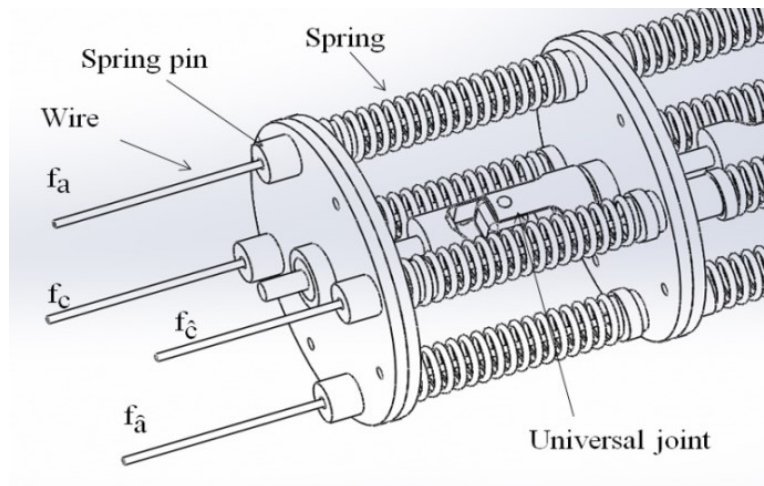
Fig. 2-5 Wire routing arrangement

As it is shown in Fig. 2-4, the first and the last discs do not slide, which means that the total length of the continuum part always remains constant. As shown in Fig.2-5, the wires pass through the inside of the springs. This wire and spring arrangement makes the wire tension vector and spring force vector almost parallel, which will avoid yielding additional torque that might occur if the two vectors are not parallel.

2.4. Pre-tension mechanism design

Pre-tension mechanism (PtM) is a passive mechanical device that compensates for wire tension in any possible posture the robot takes. The PtM device is required for the actuation system that TakoBot takes. This system uses a pair of wires driven by one motor, and multiple pairs of wires are used to control it. The PtM device might be unnecessary if one motor controls one cable individually, but such a design inevitably conduces a complexity in control.
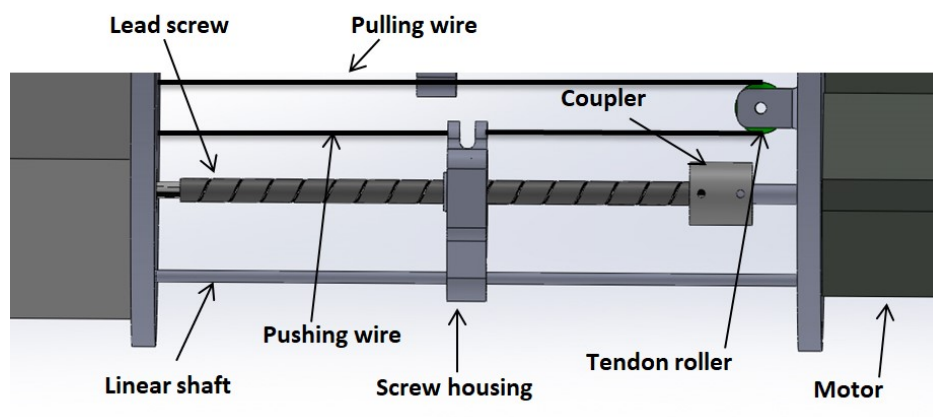
a) Paired wire actuating unit
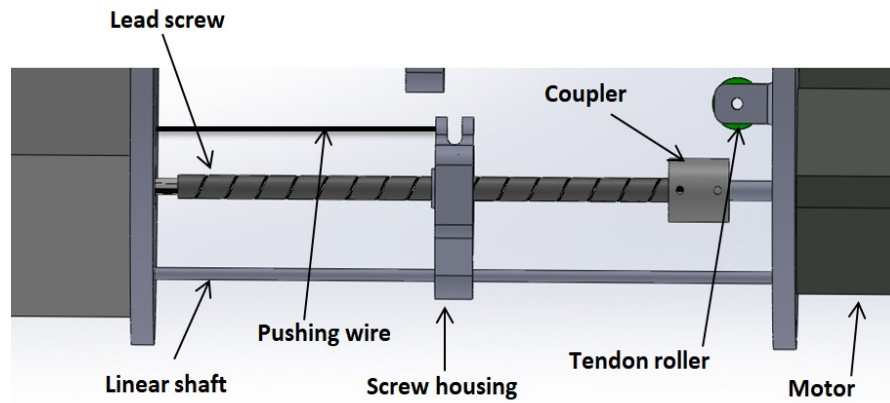
b) Single wire actuating unit

Fig. 2-6 Single and paired actuating systems

Because, all motors must be driven almost all the time during operation in order to keep a certain level of tension in every wire by monitoring tension with sensors and relaying the information back to the controller.

Also, the PtM contributes to stabilizing the motion of the manipulator by holding a certain level of tension of all wires, which avoids the sag effect.
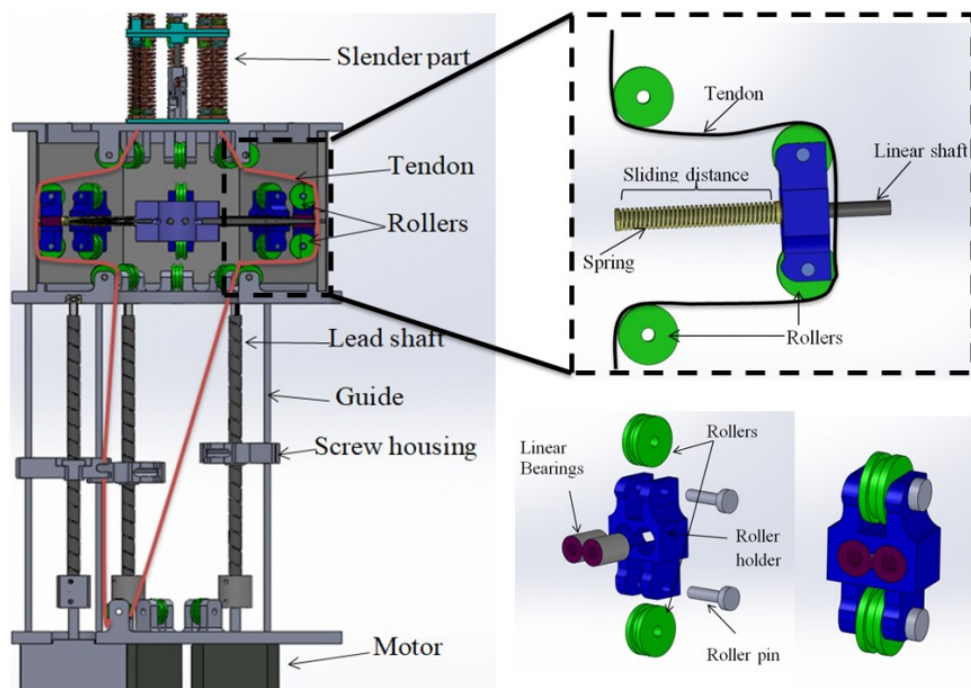

Fig. 2-7 Wire routing schematics inside the pretension mechanism

A wires passes through the PtM device, as shown in Fig. 2-7. The PtM device is equipped with rollers to prevent friction between the wire and robot parts. The PtM consists of several components: PtM holder, inner base, springs, linear guide shaft, and roller holders. The inner base is connected to the PtM holder by the linear guide shaft and the roller holder slides along the linear shaft. Wire tension is generated by compression springs along the linear shaft (Fig. 2-8 a,b). If high tension occurs on a wire, the roller holder gets close to the inner base. Thus, the PtM device can

compensate tension for eight cables simultaneously with no electronic devices being required for operation, which will enhance device reliability.
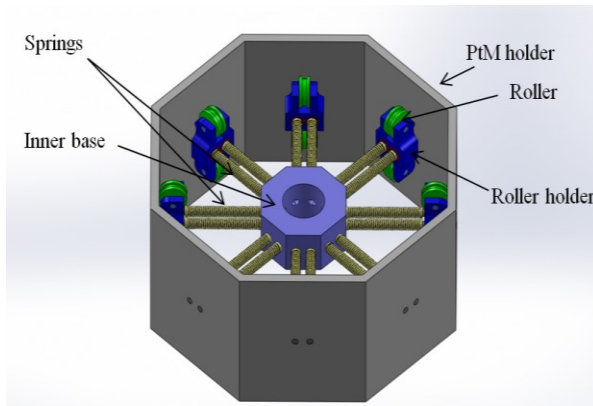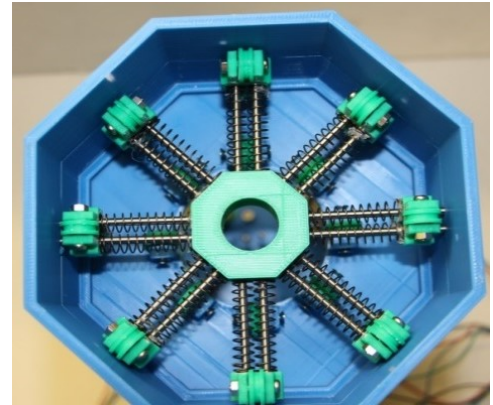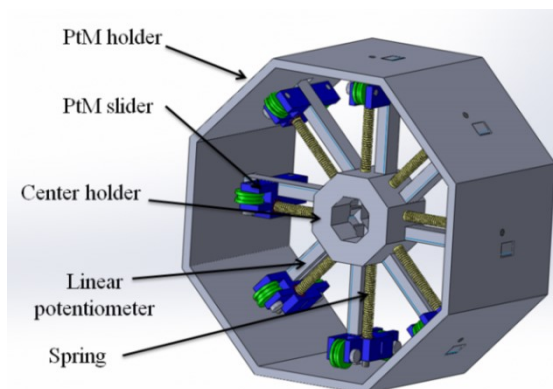

| Fig.2-8a Pretension mechanism CAD model | Fig.2-8b Fabricated prototype |

2.4.1. Hybrid pre-tension mechanism design

The pre-tension mechanism (PtM) is located in the middle part of the robot. Driving wires pass through the PtM device. The TakoBot is driven by eight wires, four wires for each section. A linear actuating unit drives wires; in this robot, one motor drives two paired wires with a strain and ease manner. A total of four motors actuate eight wires. We modified the previous design of the passive pre-tension mechanism, with equipping linear potentiometers to measure the compression length of springs for getting wire-tension feedback.

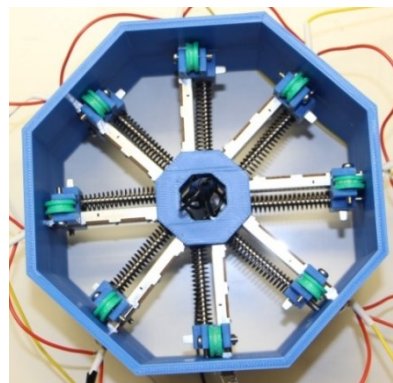Hybrid PTM CAD design   Fabricated prototype

Fig. 2-9. Hybrid pre-tension mechanism design

The previous pre-tension mechanism prototype was a fully passive mechanism to compensate wire-tension during the motion, but the new hybrid prototype represents a passive and active mechanism (see Fig.2-9) Hybrid pre-tension mechanism provides a two-level of tension compensation; firstly in a passive way, compressional spring will push the wire routing slider along the linear guide shaft. The second level intend to maintain wire-tension actively; the attached linear potentiometers provide feedback information about wire-tension to the Arduino

board, then controller sends a command to the driving motors to maintain required tension.
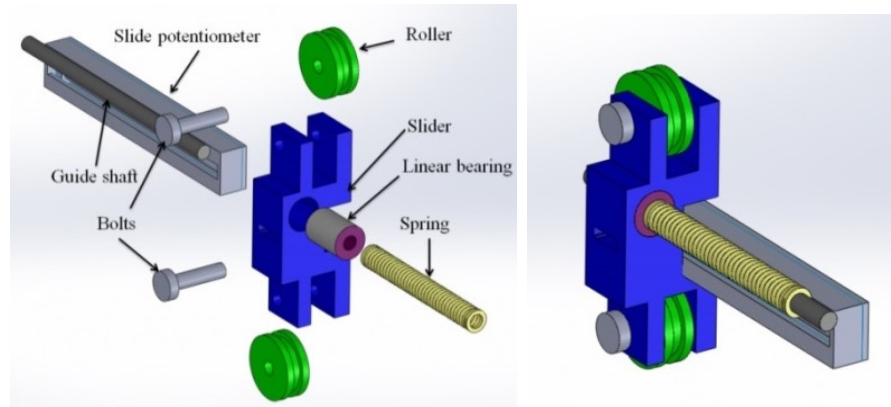

Fig. 2-10. Hybrid pre-tension mechanism wire routing slider part

2.4.2. Wire slack problems

Wire slack has a significant impact on the continuum robot rigidity and accuracy. Therefore, the proposed PtM device is important. In the process of designing pre-tension mechanism parts and selection of spring the buckling phenomenon was observed in case of using too strong springs (see Fig.2-11). Thus, after all, the spring hardness determined that PtM spring constant and segment springs constant should be close to be equal. In this case the segment spring constant is determined to 5.2 N/m and PtM spring constant is 5.1 N/m
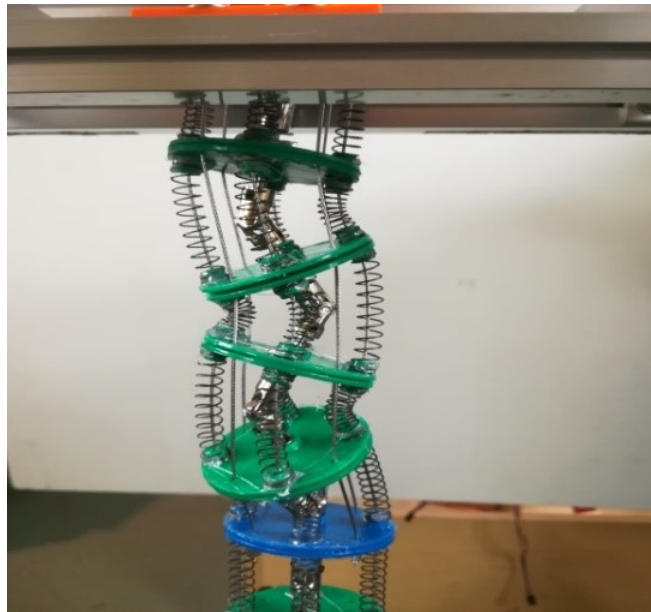

Fig.2-11. The buckling problem caused by too strong PtM springs hardness.

2.5. Actuating unit design

2.5.1. Linear actuation system

TakoBot employs long lead screw (φ 5 mm, lead 6 mm) that transfers the rotation of the individual stepping motor to the linear operation of wire. A pair of wires are actuated by one motor with strain and ease principle. Four motors are used in total: two for the first section and two other motors for the second section. As an actuating motor Hybrid Bipolar Stepping Motors with 0.49N/m torque (Trinamic Motion Control, Inc.) were used. The total shaft stroke is 150 mm. The linear guide shaft prevents the screw housing from twisting/ rotating around the screw rod (Fig. 2-12).
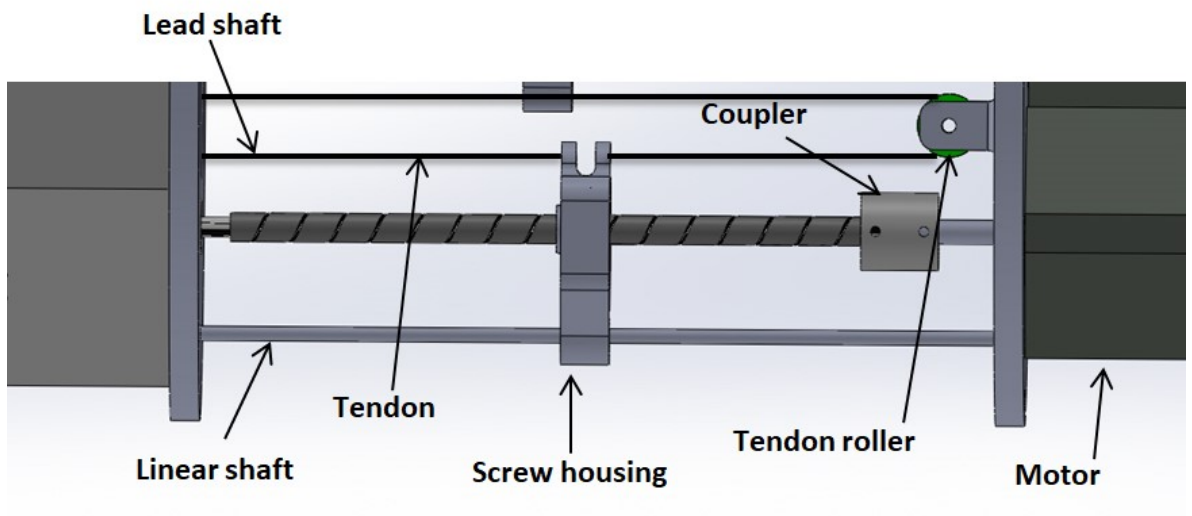

Fig.2-12 TakoBot wire actuating system

2.5.2. Pulley actuation system

In a previous prototype, we used a pulley actuating unit to control a continuum robot arm. But using pulleys brought a problem with torque, such actuation required more torque, and fixing of the wires to the pulley was not easy. The main problem was the sliding of the wires on the pulley surface (Fig 2-13).
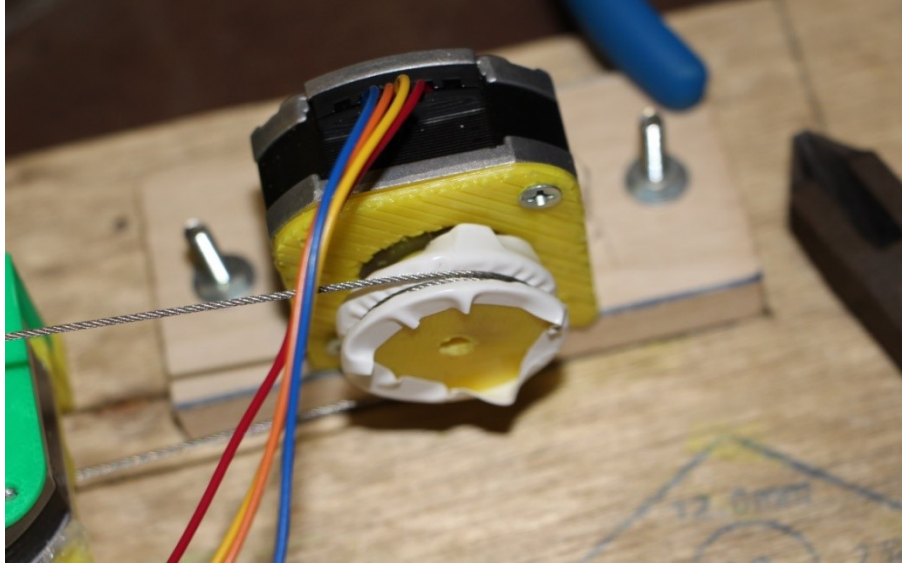

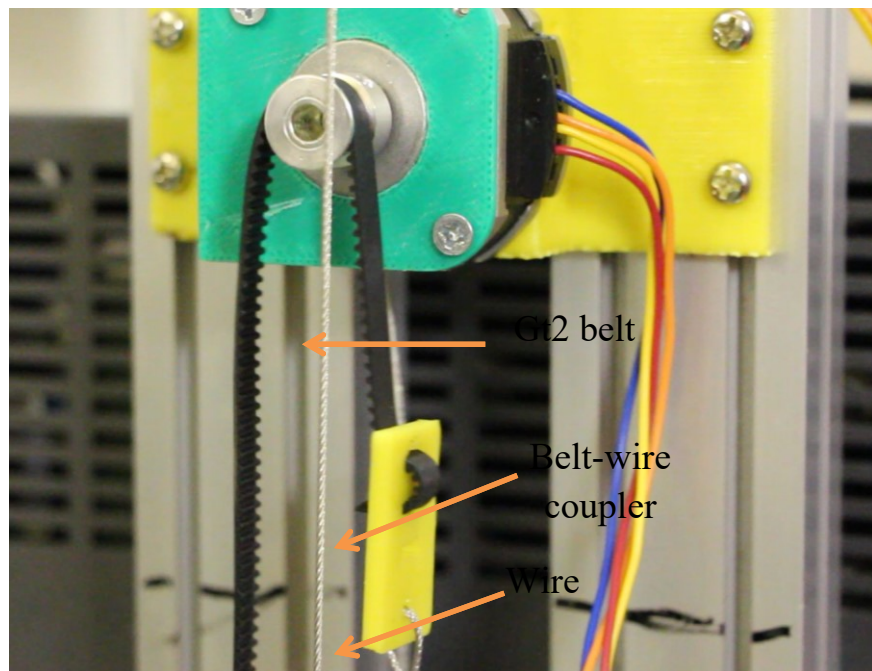Fig.2-13. Pulley actuated driving system

Fig.2-14. Driving with gt2 belt

Slipping off the wire on the pulley surface, we decided to drive wires by the gt2 belt. Driving by belt solved the problem the pulleys. Furthermore, a belt-wire coupler, belt with wires had been designed (Fig 2-14).

According to the obtained experimental results, the best wire driving was a linear driving. Thus, in our final prototype, we decided to utilize a linear driving unit.

Chapter III. KINEMATIC/KINETIC FORMULATION

There are some kinematic models for continuum manipulators describing robot structure and design in some ways. The recently published work of Sadati that is a comparative study of five methods of kinematic solutions gives a detailed explanation of models for continuum manipulators. According to this study, most discrete wire-driven continuum robots use an equivalent lumped system model, where the manipulator is a highly articulated rigid link system with a high number of links connected through universal joints or spherical joints bridged by virtual springs and a damper. In our proposed robot, we can also use such modeling to represent the actual kinematic and kinetic structures.

In this chapter, would derive equations representing the force balance between adjacent sliding discs in addition to equations describing the balance between adjacent universal joints.

Nomenclature	
Symbol	Definition
n	Total number of segments
m	Number of segments belonging to the second section
Σ_i	i-th coordinate system
$H_{i,j}$	homogeneous transformation matrix from i-th coordinate system to jth
$R_y(\theta_{yi})R_x(\theta_{xi})$	rotational matrices on y-axis and x-axis in i-th coordinate system
$u_{i-1,i}$	location of the i-th universal joint U$_i$ $(i = 1, \cdots, n-1)$ from the Σ_{i-1}
p_i	the position vector of the sliding disc
$a_i, c_i, \hat{a}_i, \hat{c}_i$	position vectors of the wire-eyelet hole (first section) $(i = 1, \cdots, n-1)$
$b_i, d_i, \hat{b}_i, \hat{d}_i$	position vectors of the wire-eyelet hole (second section) $(i = 1, \cdots, n-1)$
$f_a, f_{\hat{a}}, f_c, f_{\hat{c}}$	wire tensions of the first section
$f_b, f_{\hat{b}}, f_d, f_{\hat{d}}$	wire tension of the second section
$S_{a,i}, S_{\hat{a},i}, S_{c,i}, S_{\hat{c},i}$	the spring tension of the first section $(i = 1, \cdots, n-1)$

$S_{b,i}, S_{\hat{b},i}, S_{d,i}, S_{\hat{d},i}$	the spring tension of the second section $(i = 1, \cdots, n-1)$
m_p	is the mass of one unit including the plate, the rod and the universal joint
k	spring hardness coefficient
$\phi_a, \phi_b, \phi_c, \phi_d$	motor angles of motor-a, motor-b, motor-c and motor-d
$u_{p\sigma}, u_{p\hat{\sigma}}$	compression length of the pretension spring $(\sigma = a, b, c, d)$
k_p	the spring constant of pretension spring
λ	a lead of the screw rod
l_i	the length between neighboring universal joints $(i = 1, \cdots, n-1)$
L	Total wire length

Assumptions

(1) No friction is assumed that might occur between wires and eyelets in discs.

Wires go through the inside springs (see Fig.2-5), which will avoid any undue bending of the wire at the edge of an eyelet. It will prevent it from generating too much friction.

(2) All discs do not rotate about a backbone shaft.

Discs located at the base and the tip do not rotate (see Fig. 2-4), which means that the twisting angle of the slender part is totally zero. Therefore, the rotation of any other discs will be considered to be close to zero.

3.1. Forward kinematic formulation

Coordinate systems are set at every universal joint
The homogeneous coordinate transform matrices

$$\Sigma_0 \rightarrow \Sigma_1\colon H_{0,1} = \begin{pmatrix} R_y(\theta_{y1})R_x(\theta_{x1}) & u_{0,1} \\ 0 \quad 0 \quad 0 & 1 \end{pmatrix}, \quad u_{0,1} = \begin{pmatrix} x_0 \\ y_0 \\ l_0 \end{pmatrix} \tag{1}$$

$$\Sigma_{i-1} \rightarrow \Sigma_i\colon H_{i-1,i} = \begin{pmatrix} R_y(\theta_{yi})R_x(\theta_{xi}) & u_{i-1,i} \\ 0 \quad 0 \quad 0 & 1 \end{pmatrix} \tag{2}$$

$$u_{i-1,i} = \begin{pmatrix} 0 \\ 0 \\ L \end{pmatrix}, (i = 2, \cdots, n)$$

where $(x_0 \ y_0 \ l_0)^T$ is an initial position of the base. Two rotation matrices have:

$$R_x(\theta_{xi}) = \begin{pmatrix} 1 & 0 & 0 \\ 0 & \cos\theta_{xi} & -\sin\theta_{xi} \\ 0 & \sin\theta_{xi} & \cos\theta_{xi} \end{pmatrix}, \quad R_y(\theta_{yi}) = \begin{pmatrix} \cos\theta_{yi} & 0 & \sin\theta_{yi} \\ 0 & 1 & 0 \\ -\sin\theta_{yi} & 0 & \cos\theta_{yi} \end{pmatrix} \tag{3}$$

Multiplying the H-matrices successively, we get unit vectors and the position vector of the i-th coordinate system (Fig.3-1)
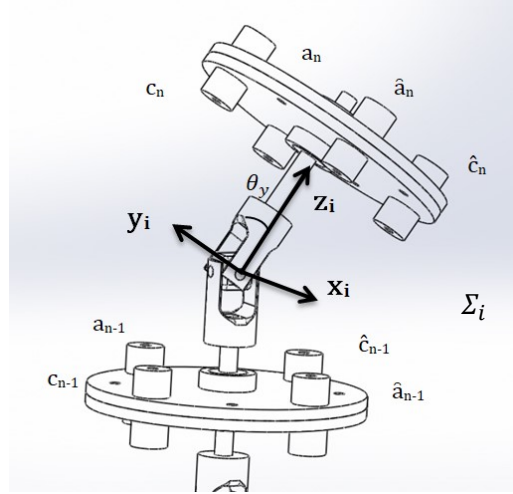

Fig.3-1 Coordinate system of i-th segment

The position vector p_i of the end-point P_n and position of sliding plates P_i ($i = 1, \cdots, n - 1$) of the manipulator are obtained by,

$$\begin{pmatrix} p_i \\ 1 \end{pmatrix} = H_{0,i}(0 \quad 0 \quad l_i \quad 1)^T, \quad (i = 1, \cdots, n) \tag{4}$$

where l_n is a fixed length between the nth universal joint and the tip plate

$$a_0 = \begin{pmatrix} a_x \\ a_y \\ 0 \end{pmatrix}, b_0 = \begin{pmatrix} b_x \\ b_y \\ 0 \end{pmatrix}, c_0 = \begin{pmatrix} c_x \\ c_y \\ 0 \end{pmatrix}, \quad d_0 = \begin{pmatrix} d_x \\ d_y \\ 0 \end{pmatrix},$$

$$\hat{a}_0 = \begin{pmatrix} \hat{a}_x \\ \hat{a}_y \\ 0 \end{pmatrix}, \quad \hat{b}_0 = \begin{pmatrix} \hat{b}_x \\ \hat{b}_y \\ 0 \end{pmatrix}, \quad \hat{c}_0 = \begin{pmatrix} \hat{c}_x \\ \hat{c}_y \\ 0 \end{pmatrix}, \quad \hat{d}_0 = \begin{pmatrix} \hat{d}_x \\ \hat{d}_y \\ 0 \end{pmatrix} \tag{5}$$

Position vectors of 4 hole are obtained as

$$\begin{pmatrix} a_i \\ 1 \end{pmatrix} = H_{0,i} \begin{pmatrix} a_x \\ a_y \\ l_i \\ 1 \end{pmatrix}, \quad \begin{pmatrix} \hat{a}_i \\ 1 \end{pmatrix} = H_{0,i} \begin{pmatrix} \hat{a}_x \\ \hat{a}_y \\ l_i \\ 1 \end{pmatrix}, \quad \begin{pmatrix} c_i \\ 1 \end{pmatrix} = H_{0,i} \begin{pmatrix} c_x \\ c_y \\ l_i \\ 1 \end{pmatrix}, \tag{6}$$

$$\begin{pmatrix} \hat{c}_i \\ 1 \end{pmatrix} = H_{0,i} \begin{pmatrix} \hat{c}_x \\ \hat{c}_y \\ l_i \\ 1 \end{pmatrix}, (i = 1, \cdots, n)$$

where l_i is an axial length between the i-th universal joint and the i-th plate, which varies as the plate slides along rods, except l_n.

In the same way, position vectors of 4-hole b, $\hat{b}_i$, d$_i$, $\hat{d}_i$ at the i-th plate $(i = 1, \cdots, m)$ are obtained as

$$\begin{pmatrix} b_i \\ 1 \end{pmatrix} = H_{0,i} \begin{pmatrix} b_x \\ b_y \\ l_i \\ 1 \end{pmatrix}, \quad \begin{pmatrix} \hat{b}_i \\ 1 \end{pmatrix} = H_{0,i} \begin{pmatrix} \hat{b}_x \\ \hat{b}_y \\ l_i \\ 1 \end{pmatrix} \tag{7}$$

$$\begin{pmatrix} d_i \\ 1 \end{pmatrix} = H_{0,i} \begin{pmatrix} d_x \\ d_y \\ l_i \\ 1 \end{pmatrix}, \quad \begin{pmatrix} \hat{d}_i \\ 1 \end{pmatrix} = H_{0,i} \begin{pmatrix} \hat{d}_x \\ \hat{d}_y \\ l_i \\ 1 \end{pmatrix}, (i = 1, \cdots, m)$$

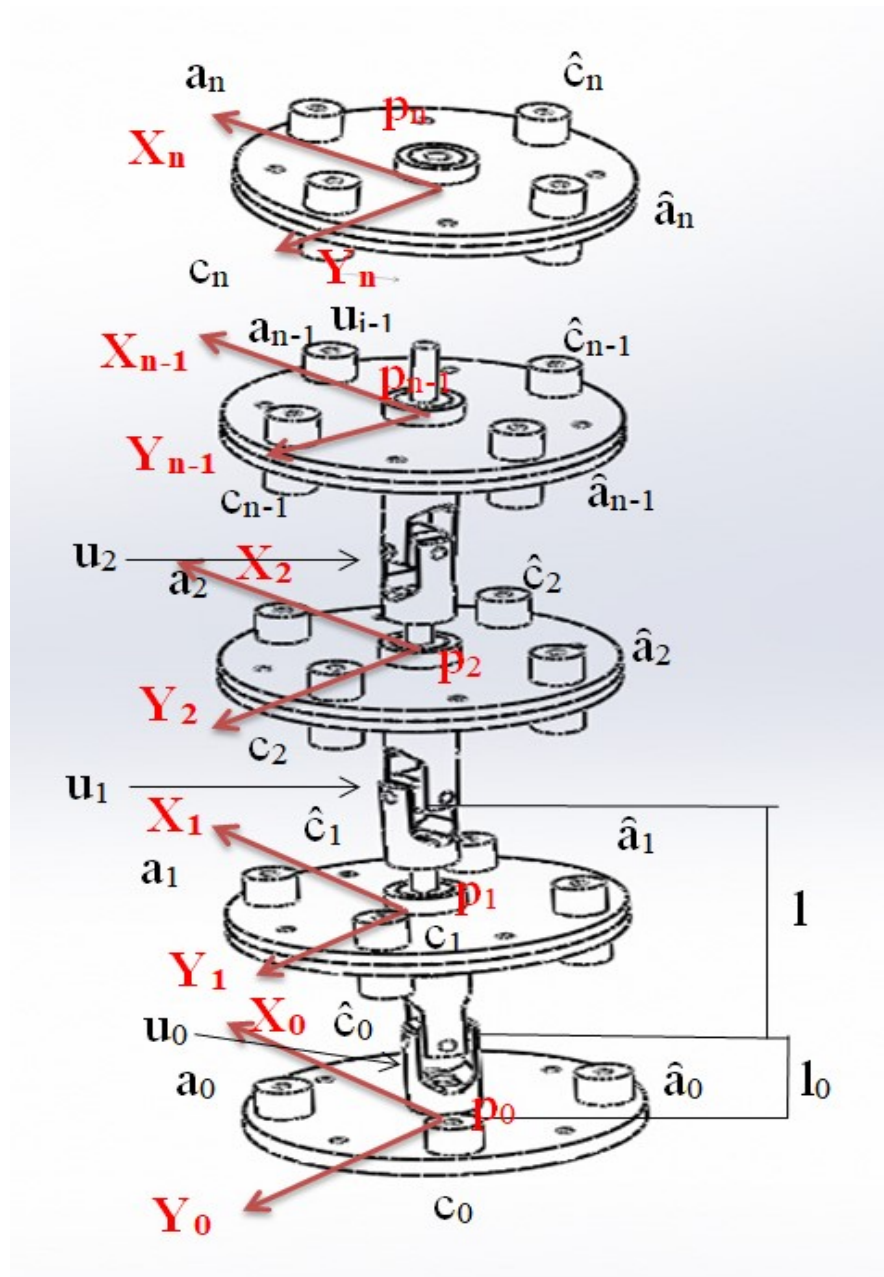Fig.3-2 TakoBot kinematic structure

3.2. Kinetic formulation

Our continuum manipulator is divided into two sections (see Fig 3-2). The first section is located near the distal part, and the second section is located near the proximal part. Two pairs of two wires operate the first section for a total of four wires. One pair of wires is controlled by one motor that pulls one wire and pushes the other wire by the same length by using the pulley. While the second section is operated by four pairs of wires for a total of eight wires. Therefore, the second section is controlled by four motors

The second section has m units, and the first section has $n-m$ units. Four pairs of wires are labeled by a and $\hat{a}$, b and $\hat{b}$, c and $\hat{c}$, d and $\hat{d}$,

Equilibrium in moments at U_n belonging to the first section is,

$$
\begin{aligned}
(S_{a,n} - f_a)\overline{(a_n - a_{n-1})} \times (a_n - u_n) + (S_{\hat{a},n} - f_{\hat{a}})\overline{(\hat{a}_n - \hat{a}_{n-1})} \\
\times (\hat{a}_n - u_n) + (S_{c,n} - f_c)\overline{(c_n - c_{n-1})} \times (c_n - u_n) \\
+ (S_{\hat{c},n} - f_{\hat{c}})\overline{(\hat{c}_n - \hat{c}_{n-1})} \times (\hat{c}_n - u_n) + m_w(p_n - u_n) \\
\times g = (0 \quad 0 \quad 0)^T
\end{aligned}
\tag{8}
$$

where $\overline{a_n - a_{n-1}} == (a_n - a_{n-1})/|a_n - a_{n-1}|$, etc. m_w is a payload applying at the end-point and g is the gravity acceleration vector.
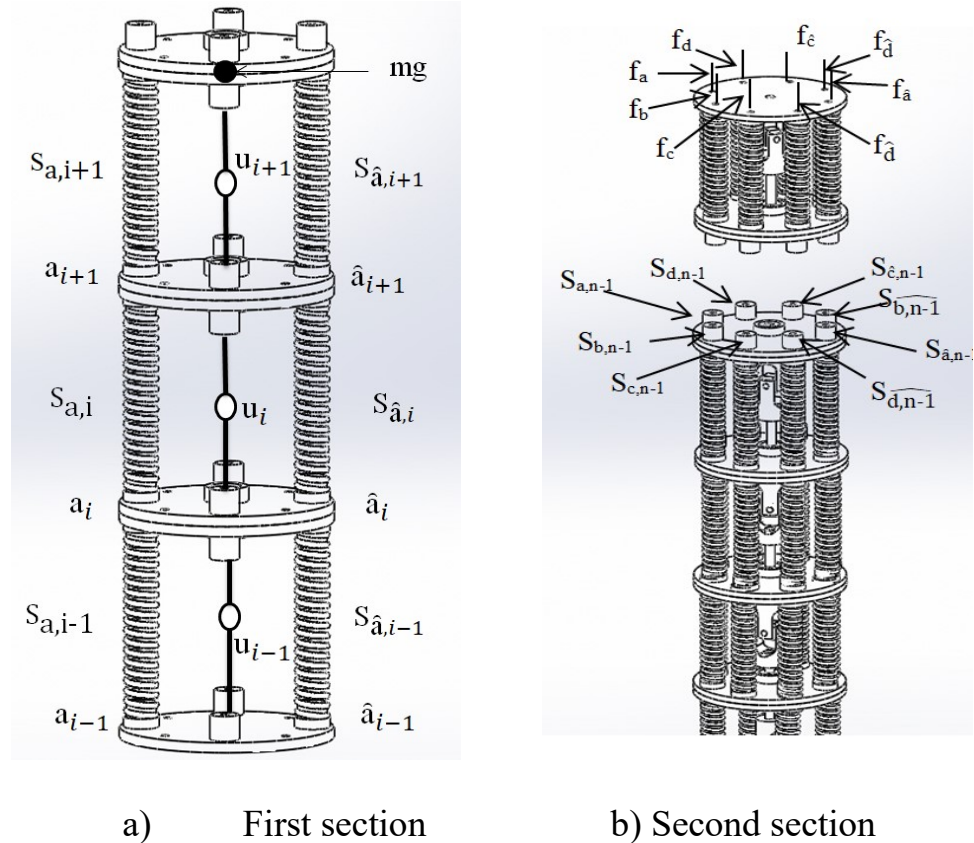

a)   First section   b) Second section

Fig.3-3 TakoBot kinetic structure

Equilibrium in moments at U_i, $(i = m+1, \cdots, n-1)$, belonging to the first section is

where f_a, $f_{\hat{a}}$, f_c, $f_{\hat{c}}$ are wire tensions, $S_{a,i}$, $S_{\hat{a},i}$, $S_{c,i}$, $S_{\hat{c},i}$, $(i = m + 1, \cdots, n)$ are spring tensions of the i-th unit. "×" means a cross product m_p is the mass of one unit including the plate, the rod and the universal joint.

$$\left(-S_{a,i+1}\overline{(a_{i+1} - a_i)} + S_{a,i}\overline{(a_i - a_{i-1})}\right) \times (a_i - u_i) +$$
$$\left(-S_{\hat{a},i+1}\overline{(\hat{a}_{i+1} - \hat{a}_i)} + S_{\hat{a},i}\overline{(\hat{a}_i - \hat{a}_{i-1})}\right) \times (\hat{a}_i - u_i) + \quad (9)$$
$$\left(-S_{c,i+1}\overline{(c_{i+1} - c_i)} + S_{c,i}\overline{(c_i - c_{i-1})}\right) \times (c_i - u_i) +$$
$$\left(-S_{\hat{c},i+1}\overline{(\hat{c}_{i+1} - \hat{c}_i)} + S_{\hat{c},i}\overline{(\hat{c}_i - \hat{c}_{i-1})}\right) \times (\hat{c}_i - u_i) + \left(m_w(p_n - u_i) + m_p \sum_{k=i+1}^{n-1}(p_k - u_i)\right) \times g = (0 \quad 0 \quad 0)^T$$

$$S_{a,i} = k(L - |a_i - a_{i-1}|), S_{\hat{a},i} = k(L - |\hat{a}_i - \hat{a}_{i-1}|), \quad (10)$$
$$S_{c,i} = k(L - |c_i - c_{i-1}|), \quad S_{\hat{c},i} = k(L - |\hat{c}_i - \hat{c}_{i-1}|),$$

with the spring coefficient k. Equations (8) and (9) contain $3(n-m)$ equations including $4(n-m)-1$ variables of the $n-m$ universal joints angles θ_{xi}, θ_{yi}, θ_{zi}, $(i = m + 1, \cdots, n)$ and slide length of plates l_i $(i = m + 1, \cdots, n - 1)$.

The spring tensions are obtained as,

Equilibrium in force at i-th plate $(i = m + 1, \cdots, n - 1)$ is,

$$\left(-S_{a,i+1}\overline{(a_{i+1} - a_i)} + S_{a,i}\overline{(a_i - a_{i-1})} - S_{\hat{a},i+1}\overline{(\hat{a}_{i+1} - \hat{a}_i)}\right.$$
$$+ S_{\hat{a},i}\overline{(\hat{a}_i - \hat{a}_{i-1})} - S_{c,i+1}\overline{(c_{i+1} - c_i)} \quad (11)$$
$$+ S_{c,i}\overline{(c_i - c_{i-1})} - S_{\hat{c},i+1}\overline{(\hat{c}_{i+1} - \hat{c}_i)} + S_{\hat{c},i}\overline{(\hat{c}_i - \hat{c}_{i-1})} + (n$$
$$\left. - i)\, m_p g\right) \cdot (p_i - u_i) = 0$$

Equation (11) provides $n-m-1$ equations. Combined it with (8) and (9), we obtain $4(n-m)-1$ equations, which suffices in number to solve for $4(n-m)-1$ variables; $\theta_{x,i}$, $\theta_{y,i}$, $\theta_{z,i}$ $(i = m + 1, \cdots, n)$ and l_i $(i = m + 1, \cdots, n - 1)$ for a given set of wire tensions f_a, $f_{\hat{a}}$, f_c, $f_{\hat{c}}$.

Equilibrium in moments at U_m, the universal joint located at the most distal position belonging to the second section is

$$-S_{a,m+1}\overline{(a_{m+1} - a_m)} \times (a_m - u_m) + (S_{b,m} - f_b)\overline{(b_m - b_{m-1})}$$
$$\times (b_m - u_m)$$
$$- S_{\hat{a},m+1}\overline{(\hat{a}_{m+1} - \hat{a}_m)} \times (\hat{a}_m - u_m) + (S_{\hat{b},m} - f_{\hat{b}})\overline{(\hat{b}_m - \hat{b}_{m-1})} \quad (12)$$
$$\times (\hat{b}_m - u_m)$$
$$-S_{c,m+1}\overline{(c_{m+1} - c_m)} \times (c_m - u_m) + (S_{d,m} - f_d)\overline{(d_m - d_{m-1})}$$
$$\times (d_m - u_m)$$
$$-S_{\hat{c},m+1}\overline{(\hat{c}_{m+1} - \hat{c}_m)} \times (\hat{c}_m - u_m) + (S_{\hat{d},m} - f_{\hat{d}})\overline{(\hat{d}_m - \hat{d}_{m-1})}$$
$$\times (\hat{d}_m - u_m)$$
$$+ \left(m_w(p_n - u_m) + m_p \sum_{k=m+1}^{n-1}(p_k - u_m)\right) \times g = (0 \quad 0 \quad 0)^T$$

For the second segment, we can derive similar equations as (9), (10) and (11) by replacing $\{a_i, \hat{a}_i, c_i, \hat{c}_i\}$ with $\{b_i, \hat{b}_i, d_i, \hat{d}_i\}$, $\{S_{a,i}, S_{\hat{a},i}, S_{c,i}, S_{\hat{c},i}\}$ with $\{S_{b,i}, S_{\hat{b},i}, S_{d,i}, S_{\hat{d},i}\}$ for $i = 1, \cdots, m-1$ in (10) and for $i = 1, \cdots, m$ in (10) and (11).

As a result, we obtain $4m$ equations included by Equation (12), which suffices in number to solve for $4m$ variables; $\theta_{x,i}$, $\theta_{y,i}$, $\theta_{z,i}$ and l_i ($i = 1, \cdots, m$) for a given set of wire tensions f_b, $f_{\hat{b}}$, f_d, $f_{\hat{d}}$.

Wire tensions f_a, $f_{\hat{a}}$, f_c, $f_{\hat{c}}$, f_b, $f_{\hat{b}}$, f_d, $f_{\hat{d}}$ are determined according to 4 motors' angles $\phi_a, \phi_b, \phi_c, \phi_d$ (Fig 3-4)
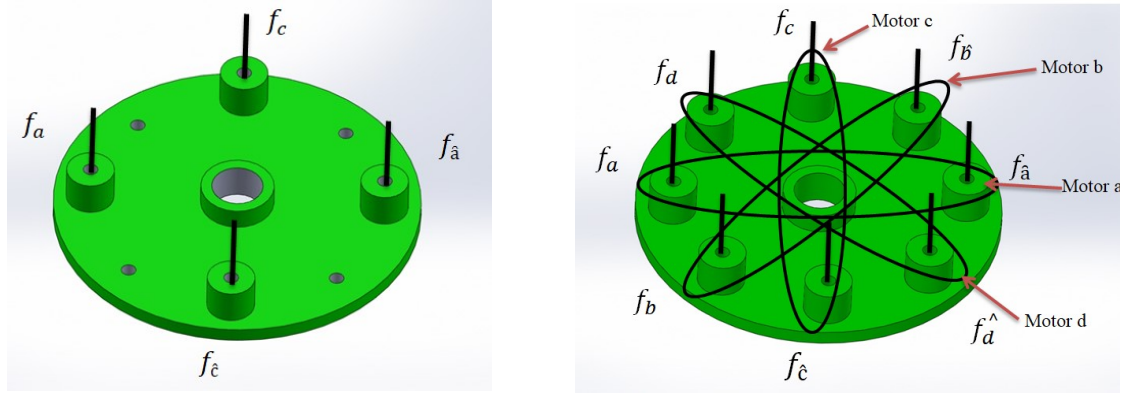
First section spacer disc   Second section spacer disc

Fig.3-4 Wire eyelet arrangement on the disc

3.3. Pre-tention mechanism formulation

Fig.3-5 shows a model of the pre-tension mechanism
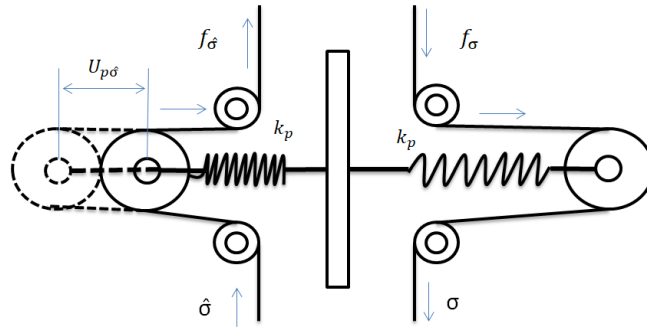
Fig.3-5 Pre-tension mechanism nomenclature

The pretension spring receives $2f$, therefore:

$$2f_\sigma = k_p u_{p\sigma}, \ (\sigma = a, b, c, d), \quad 2f_{\hat{\sigma}} = k_p u_{p\hat{\sigma}}, \ (\hat{\sigma} = \hat{a}, \hat{b}, \hat{c}, \hat{d}) \quad (13)$$

where $u_{p\sigma}$ and $u_{p\hat{\sigma}}$ are determined by motor rotation angle and wire length

$$2u_{p\sigma} = 2\bar{u}_{p\sigma} + \frac{\lambda\varphi_\sigma}{2\pi} + \sum_{i=1}^{n}|\sigma_i - \sigma_{i-1}| - nL, \quad 2u_{p\hat{\sigma}} = 2\bar{u}_{p\hat{\sigma}} - \frac{\lambda\varphi_\sigma}{2\pi} + \sum_{i=1}^{n}|\hat{\sigma}_i - \hat{\sigma}_{i-1}| - nL \quad (14)$$

where $2\bar{u}_{p\sigma}$ and $2\bar{u}_{p\acute{\sigma}}$ are compression length of the pretension spring, which are preset initially.

Substituting Equation (14) into Equation (13), we have;

$$f_a = \frac{1}{2}k_p\left(2\bar{U}_{pa} + \frac{\lambda\phi_a}{4\pi} + \frac{1}{2}\left(\sum_{i=1}^{n}|a_i - a_{i-1}| - nL\right)\right),$$

$$f_{\hat{a}} = \frac{1}{2}k_p\left(2\bar{U}_{p\hat{a}} - \frac{\lambda\phi_a}{4\pi} + \frac{1}{2}\left(\sum_{i=1}^{n}|\hat{a}_i - \hat{a}_{i-1}| - nL\right)\right)$$

$$f_c = \frac{1}{2}k_p\left(2\bar{U}_{pc} + \frac{\lambda\phi_c}{4\pi} + \frac{1}{2}\left(\sum_{i=1}^{n}|c_i - c_{i-1}| - nL\right)\right), \qquad (15)$$

$$f_{\hat{c}} = \frac{1}{2}k_p\left(2\bar{U}_{p\hat{c}} - \frac{\lambda\phi_{\hat{c}}}{4\pi} + \frac{1}{2}\left(\sum_{i=1}^{n}|\hat{c}_i - \hat{c}_{i-1}| - nL\right)\right)$$

$$f_b = \frac{1}{2}k_p\left(2\bar{U}_{pb} + \frac{\lambda\phi_b}{4\pi} + \frac{1}{2}\left(\sum_{i=1}^{n}|b_i - b_{i-1}| - nL\right)\right),$$

$$f_{\hbar} = \frac{1}{2}k_p\left(2\bar{U}_{p\hbar} - \frac{\lambda\phi_{\hbar}}{4\pi} + \frac{1}{2}\left(\sum_{i=1}^{n}|\hbar_i - \hbar_{i-1}| - nL\right)\right)$$

$$f_d = \frac{1}{2}k_p\left(2\bar{U}_{pd} + \frac{\lambda\phi_d}{4\pi} + \frac{1}{2}\left(\sum_{i=1}^{n}|d_i - d_{i-1}| - nL\right)\right),$$

$$f_{\hat{d}} = \frac{1}{2}k_p\left(2\bar{U}_{p\hat{d}} - \frac{\lambda\phi_{\hat{d}}}{4\pi} + \frac{1}{2}\left(\sum_{i=1}^{n}|\hat{d}_i - \hat{d}_{i-1}| - nL\right)\right)$$

3.4. Inverse kinematic formulation

According to the given set of variables $\theta_{x,i}$, $\theta_{y,i}$, $\theta_{z,i}$ $(i = 1, \cdots, n)$ and l_i $(i = 1, \cdots, n-1)$, would calculate the end-point position by Equation (4),

$$\begin{pmatrix} p_n \\ 1 \end{pmatrix} = H_{0,n} \begin{pmatrix} 0 \\ 0 \\ l_n \\ 1 \end{pmatrix} = \begin{pmatrix} i_n & j_n & k_n & r_n \\ 0 & 0 & 0 & 1 \end{pmatrix} \begin{pmatrix} 0 \\ 0 \\ l_n \\ 1 \end{pmatrix} = \begin{pmatrix} k_n l_n + r_n \\ 1 \end{pmatrix} \qquad (16)$$

Taking a total differentiation of $p_n = k_n l_n + r_n$ with respect to $\theta_{x,i}$, $\theta_{y,i}$, $\theta_{z,i}$ $(i = 1, \cdots, n)$ and l_i $(i = 1, \cdots, n-1)$ and also motor angles ϕ_a, ϕ_b, ϕ_c, ϕ_d,

$$\Delta p_n = \frac{\partial p_n}{\partial v} \Delta v + \frac{\partial p_n}{\partial \phi} \Delta \phi \qquad (17)$$

where $\quad v = (\theta_{x1}, \theta_{x2}, \cdots, \theta_{xn}, \theta_{y1}, \theta_{y2}, \cdots, \theta_{yn} \cdots, l_1, l_2, \cdots, l_{n-1}) \in \mathcal{R}^{4n-1}$ and

$\phi = (\phi_a, \phi_b, \phi_c, \phi_d)$. $\frac{\partial p_n}{\partial v} \in \mathcal{R}^{3 \times 4n-1}$ and $\frac{\partial p_n}{\partial \phi} \in \mathcal{R}^{3 \times 4}$.

Let $w = (w_1, w_2, \cdots w_{4n-1})^T = 0_{4n-1}$ represents the 4n-1 equations provided by Equations (8–11), which also includes $\theta_{x,i}$, $\theta_{y,i}$, $(i = 1, \cdots, n)$, l_i $(i = 1, \cdots, n-1)$ and also motor angles ϕ_a, ϕ_b, ϕ_c, ϕ_d.

Taking a total differentiation for $w = (w_1, w_2, \cdots w_{4n}) = 0_{4n-1}$ as well, we have,

$$\Delta w = \frac{\partial w}{\partial v} \Delta v + \frac{\partial w}{\partial \phi} \Delta \phi = 0_{4n-1} \qquad (18)$$

where $\frac{\partial w}{\partial v} \in \mathcal{R}^{(4n-1) \times (4n-1)}$ and $\frac{\partial w}{\partial \phi} \in \mathcal{R}^{(4n-1) \times 4}$. Since $\frac{\partial w}{\partial v}$ is a square matrix, we can solve Equation (20) with respect to the vector Δv as,

$$\Delta v = -\left(\frac{\partial w}{\partial v}\right)^{-1} \frac{\partial w}{\partial \phi} \Delta \phi \qquad (19)$$

Substituting Equation (17) into Equation (15), we have

$$\Delta p_n = -\frac{\partial p_n}{\partial v}\left(\frac{\partial w}{\partial v}\right)^{-1} \frac{\partial w}{\partial \phi} \Delta \phi + \frac{\partial p_n}{\partial \phi} \Delta \phi = \left(\frac{\partial p_n}{\partial \phi} - \frac{\partial p_n}{\partial v}\left(\frac{\partial w}{\partial v}\right)^{-1} \frac{\partial w}{\partial \phi}\right) \Delta \phi \qquad (20)$$
$$= J \Delta \phi$$

which can be solved for $\Delta \phi$, by using a generalized inverse of the Jacobian $J \in \mathcal{R}^{3 \times 4}$

$$\Delta \phi = J^\dagger \Delta p_n + P^\perp (J) \Delta \phi_N \qquad (21)$$

where $J^\dagger \in \mathcal{R}^{4 \times 3}$ is a generalized inverse of J and $P^\perp(J) \in \mathcal{R}^{4 \times 4}$ is a null projection operator of J, and $\Delta \phi_N \in \mathcal{R}^4$ is a correction of ϕ so as to minimize a positive scalar potential φ by making use of a redundant actuation. We use $J^\dagger = J^T (J J^T)^{-1}$ and $P^\perp(J) = I - J^\dagger J$.

Equation (19) provides a variation of motor angles $\Delta \phi$ for a given position and direction variation Δp_n.

3.5. Kinematics simulation and analysis

The simulation studies were done for the following purposes.

(1) To validate the formulations described in the former section.

(2) To validate the effect of disc sliding by comparing cases of sliding discs and non-sliding discs.

Due to the limitations of computer memory capacity, we confined the number of segments to 4 in the first section and 3 in the second section (the actual Takobot has 4 and 5, respectively). Therefore, the total number of segments n is 7, and the total number of equations $3n$-1 is 20. Table 3-1 shows the physical parameters used in the simulation.

Table 3-1. Values used for the simulation

Ls	The natural length of spring	60[mm]
ks	Spring constant of the springs between UJs	0.8 [N/mm]
kp	Spring constant of the pretension springs	1.6 [N/mm]
m_w	Payload	0 [kg]
lp	Pulling length to yield pretension	30 [mm]
gz	Gravity acceleration	9.80665[mm/s^2]
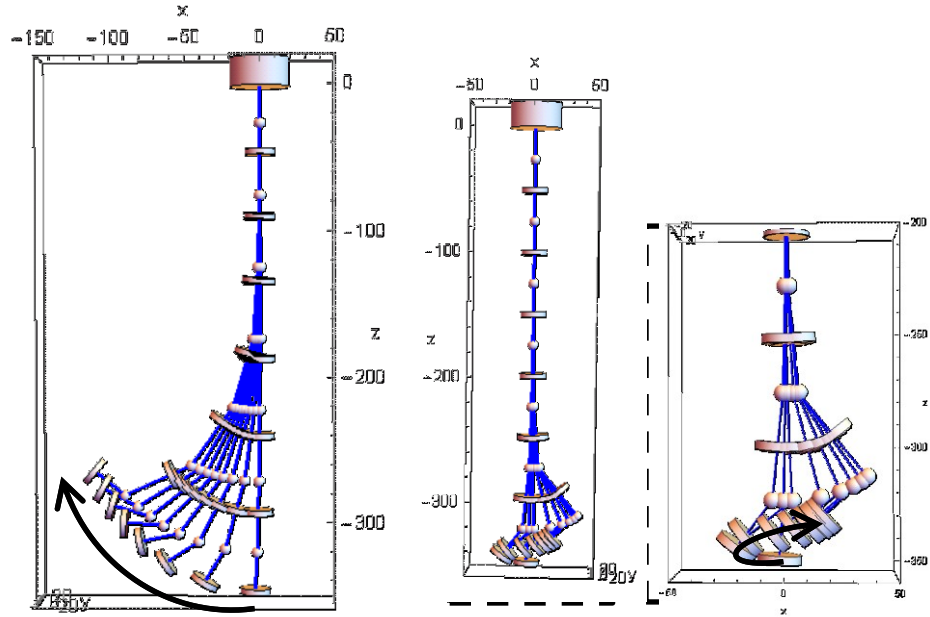
(a) the case of sliding discs   (b) the case of non-sliding discs

Fig.3-7 Simulation results when only the motor-a rotates 6 revolution

It observes the motion of the TacoBot when only motor-a rotates 12π[rad] (6 [rev]) at a constant rate. It aims to compare motions between the disc sliding and non-sliding. Newton's method was employed several times to converge 20 equations close to being zero with the specified motor angles. Fig.3-7 shows the motion of the TakoBot. Small spheres represent universal joints. The springs located between adjacent discs are not drawn. As shown in Fig.3-7, the end-plate takes a monotonical movement with the monotonical rotation of the motor-a in the case of disc sliding. It's desirable for control. However, the end-plate takes back and forth motion with the same rotation of motor-a in the case of the non-sliding disc. It is due to a high-bending torque yielded at the last universal joint. This non-monotonically response will make the control difficult. In the case of the real application, applied motor torque concentrates on the bending joint, which causes more friction interference between the wire and spacer disc eyelets. Thus, the non-sliding prototype consumes more power as well.
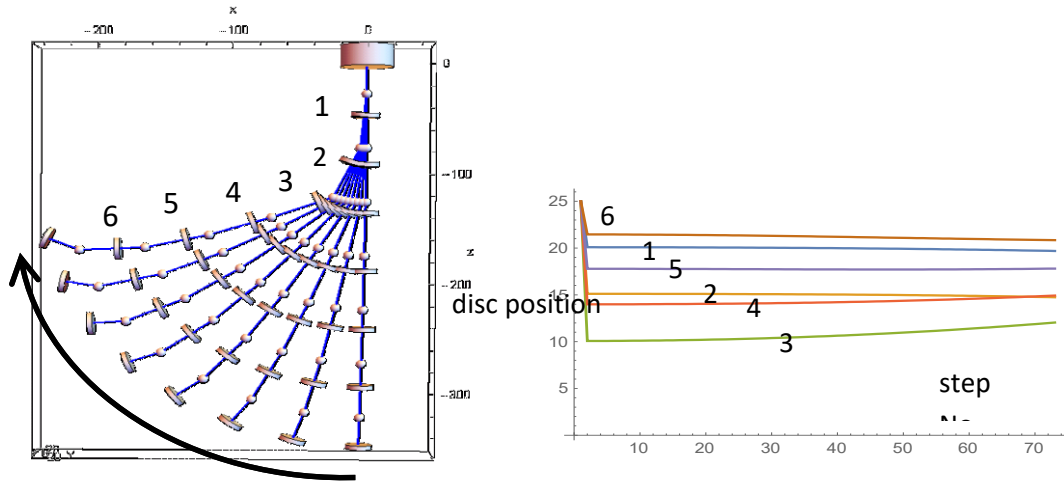
(a) Motion of Takobot   (b) Positions of discs (length from the former UJ)

Fig.3-8 Simulation results when the motor-a and motor-c rotates 6 rotations and the motor-d rotates for the case of sliding disc -6 revolutions simultaneously

Fig.3-8 (a) shows the motion of the TakoBot when motor-a and motor-c rotate 12π[rad] (6 [rev]) and motor-d rotates -12π[rad] (-6 [rev]) at a constant rate. Fig.3-8(b) shows the sliding length of the discs during the motion. The initial positions of all discs are 25 [mm]. At first, all of them slide largely because the specified pre-tension is assumed to be loaded at the first step.
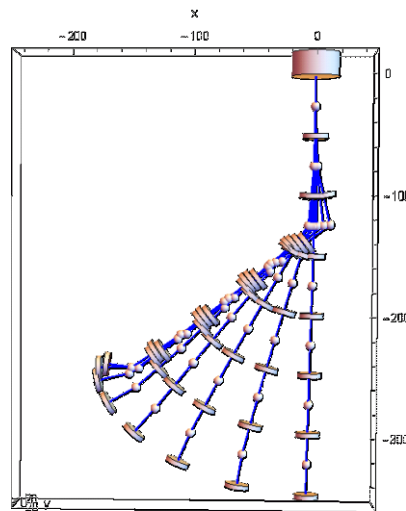
Fig.3-9. Simulation results for the case of non-sliding discs when motor-a and motor-c rotates 6 rotations and motor-d rotates -6 revolutions simultaneously

Fig.3-9 shows the motion of the prototype with non-sliding discs when the

35

motors rotate in the same way as shown in Fig.3-8. As shown, the tip of the manipulator lifts up less than the case of sliding discs. This phenomenon is the same as those observed in the actual experiment shown in Fig.3-9. Also, it is observed that two joints driven by wires directly rotate largely, which is the same phenomenon as those observed in the actual experiment shown in Fig.3-10 and 3-11.

Moreover, to validate the formulation of control, we created the following task: move the end-effector disc 50 mm along the z-axis and x-axis by 50 steps (Fig 3-10, 11) (1 mm at every step). Eq. (21) without null-projection term is used. To visualize the motion of the manipulator, we used three motors to get a visual result on a two-dimensional plane (X-Z). TakoBot's four motors are labeled as motor a, motor b, motor c, and motor d. The first two motors are for actuating the first section, and the other two motors are for the second section actuation. In this simulation, we actuated motor a, motor b, and motor d. Motor c mostly remains at zero. This is for manipulator motion on the X-Z plane.

Main view   Zoom view

Disc position   Motor angles (motor-a,b,c,d)
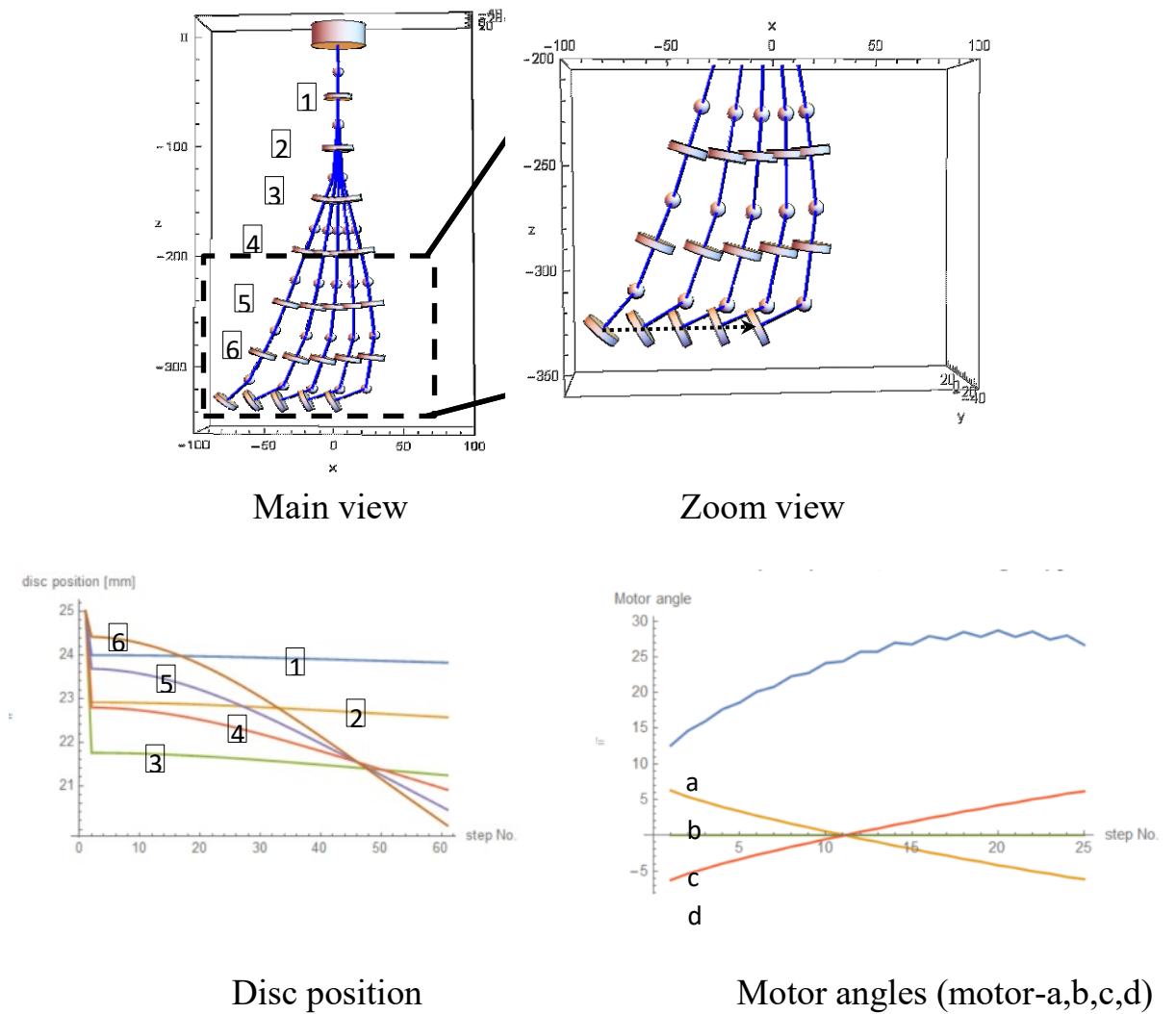
Fig. 3-10 The end-effector moves straight upward along X-axis 50 mm.
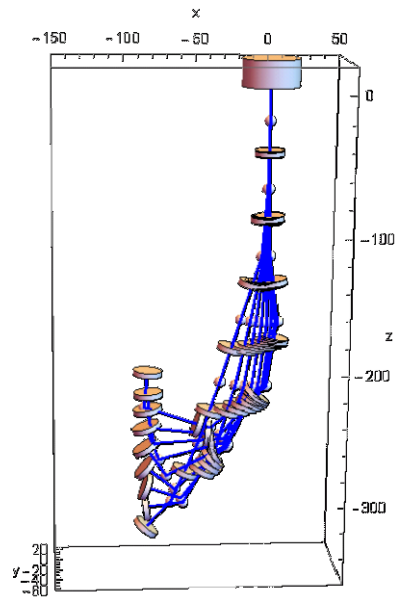
Main view   Zoom view
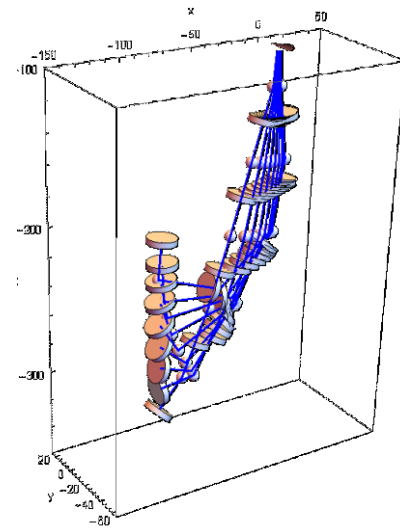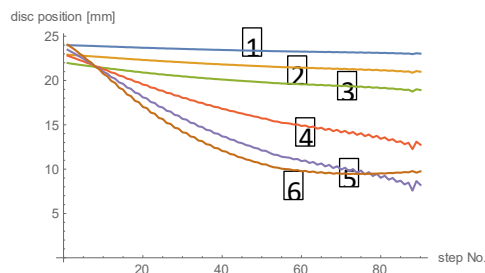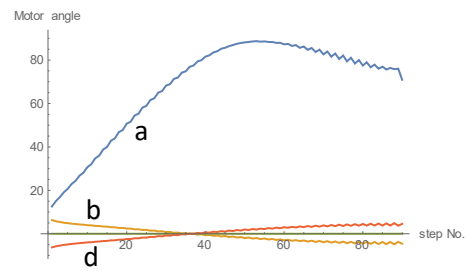
Disc position   Motor angles

Fig.3-11 The end-point moves straight upward along Z-axis 130 mm.

According to the obtained results, the sliding backbone disc mechanism engages several segments bending, while the non-sliding backbone bends the actuating segment greatly (Fig.3-11).

Chapter IV ROBOT CONTROL

This chapter deals with the wire-driven continuum robot control. Also this chapter explains two main control methods of TakoBot: teleoprated control and compensative driving control method. The chapter is organized on following order: robot control architecture, wire tension feedback control, test on payload capacity, test on basic motions and natural frequency test.

4.1. Robot control architecture

A standard teleoperated controller using two joystick is employed to control the TakoBot. According to the robot design, the manipulator has total four motors ; two motors for controlling the section 1 and the other two for the section two. As an actuating unit, bipolar stepping motors with 0.69Nm torque were used. The motor driver is TMC 2208 from (Trinamic Motion INC). The controller is Arduino UNO (see Table4-1).

Table 4-1. Components of the controller

#	Component	Manufacturer	Pcs
1	Arduino Uno	Arduino	1
2	Stepping motor QSH4218	Trinamic motion INC	4
3	Motor driver TMC2208	Trinamic motion INC	4
4	Joystick 2 axis	Adafruit	2
5	Springs WR8-35	Misumi Vona	40
6	Springs WR5-40	Misumi Vona	16
7	Linear bearings CLMU-3	Misumi Vona	26
8	Linear shaft SFJ3-400	Misumi Vona	5
9	Wires	Adafruit	50m
10	Cooler	Sanyo denki	1
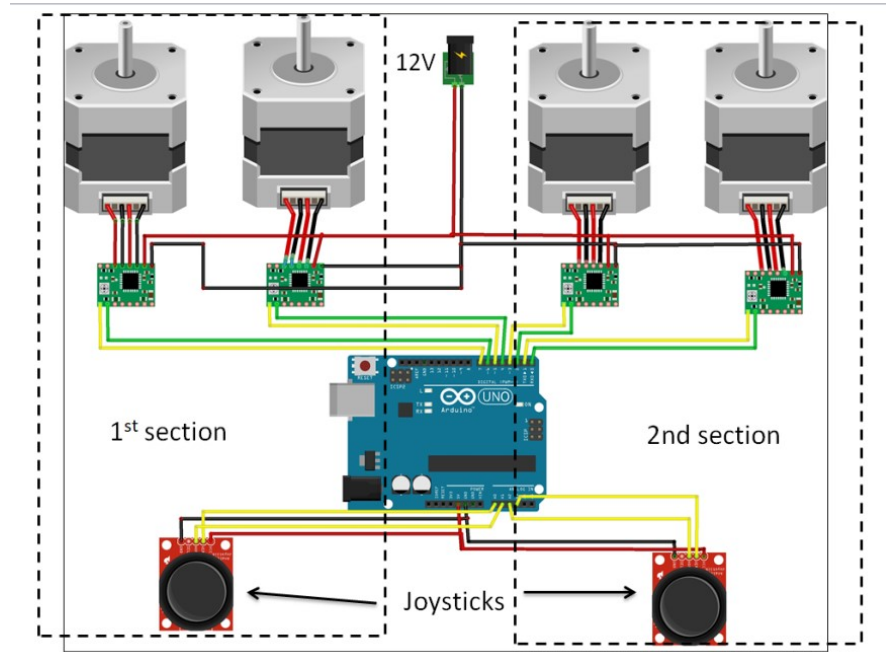
Fig.4-1. Takobot control schematics

Fig. 4-1 shows that control schematics and control board wiring. The motor drivers and stepping motors consume 12V, Arduino board and joysticks consumes six voltages. For a long time working, it included a cooler fan additionally.

Motion starts from the joysticks; it gives the desired driving direction to the motors. In general, the robot can move in four directions: up, down, left, and right. Those primitive motions are enough to reach the desired position. However, due to existing 2 actuated sections, based on robot wire arrangement design, it makes the control process complicated. The first section wires are located with the 90-degree arrangement, coincident with x and y–axes, but the second section wires aligned in 45 degrees inclined with x and y–axes (see Fig.4.2), which means corporative operation of first and second sections are required. Moreover, both sections cannot be controlled with a single joystick because the robot should do 'S' shape motions to improve the reachability of the manipulator, which is possible only with cooporative operation of the two joysticks.
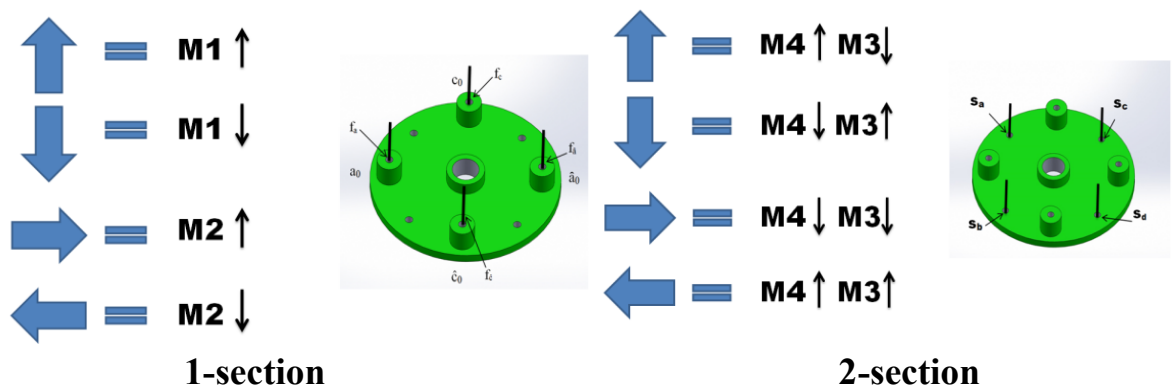
1-section   **2-section**

Fig.4-2. Control arrangement

Fig. 4-2 shows that the control of the first section is simple, but the the control of the second section requires a combined control method. Here M1, M2, M3, and

M4 are motors. In Fig.4-2, the blue arrows show desired motion direction of the end-point, the black arrows show motor driving direction; up–clockwise, down–counter-clockwise. The discs shows the wires arrangent on the disc, for first and second sections. So, the first section wires alingned on 90 degree from each other, but the second section wires alined in 45 degrees from the first section wires. Therefore, 2nd section wires control is more complex.

Fig.4-3. Takobot shape control combinations.

Based on control combinations, the desired robot postures and shapes can be obtained as shown in Fig 4-3, in which the blue arrows near the joysticks shows the button push directions to reach the required shapes of the continuum part as shown in the left column.

TakoBot is actuated by eight wires, for the first section two motors drive paired wires; motor-A drives paired wires $a, \hat{a}$ and motor-C drives paired wires $c, \hat{c}$. The second section actuation is similar, motor-B drives paired wires b and $\hat{b}$, while motor-D drives paired wires d and $\hat{d}$ (see Fig.4-5). The purpose of the proposed control strategy is to actuate the wires simultaneously. This means that in the case of a robot having only a single actuated section, wire-tension and robot accuracy are easy to predict. Still, in case actuating of multi-section, we might face with wire

slack and control accuracy problem. Such issues occur because a driving of a section might change wire-tensions of the neighboring section as well.
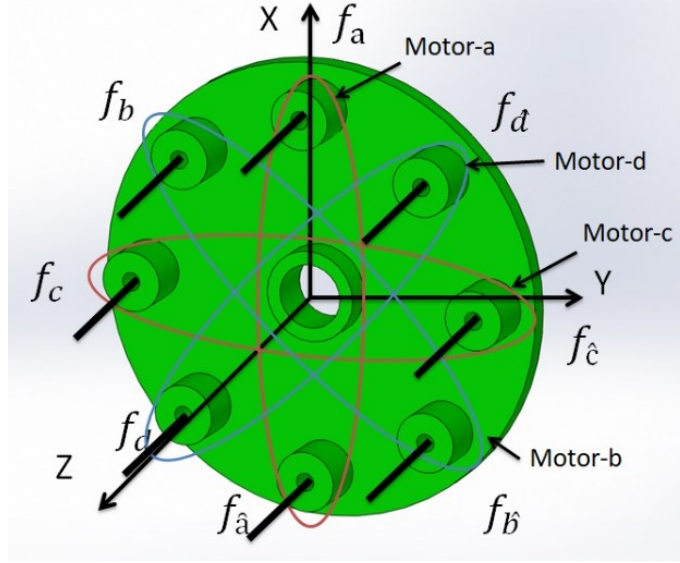

Fig.4-5. Motor and wire arrangements

4.2. Control strategy

Based on this wire-allocation, we propose a control strategy with instinctive hybrid ways simultaneously operated.

(1) **Primitive driving (P-driving)**: 4 motors are driven according to the previously determined operations of the two joysticks to achieve typical shapes of the manipulators shown in Fig.4-3.

(2) **Compensatory driving (C-driving)**: The above primitive driving will induce a deviation along the vertical axis or might yield wire-slacking, which should be compensated in actual works of the manipulator. For example, the manipulator will take a load at the end-point, which will move the end-point downward, which should be compensated.

It follows to formulate the compensatory driving denoted below.

The pre-tension spring receives $2f$ (see Fig.4-6), therefore:

$$2f_\sigma = k_p u_{p\sigma}, \ (\sigma = a, b, c, d)$$
$$2f_{\hat{\sigma}} = k_p u_{p\hat{\sigma}}, \ (\hat{\sigma} = \hat{a}, \hat{b}, \hat{c}, \hat{d}) \tag{22}$$

where $u_{p\sigma}$, $u_{p\hat{\sigma}}$ are compression length of the pretension spring of which spring constant is k_p.
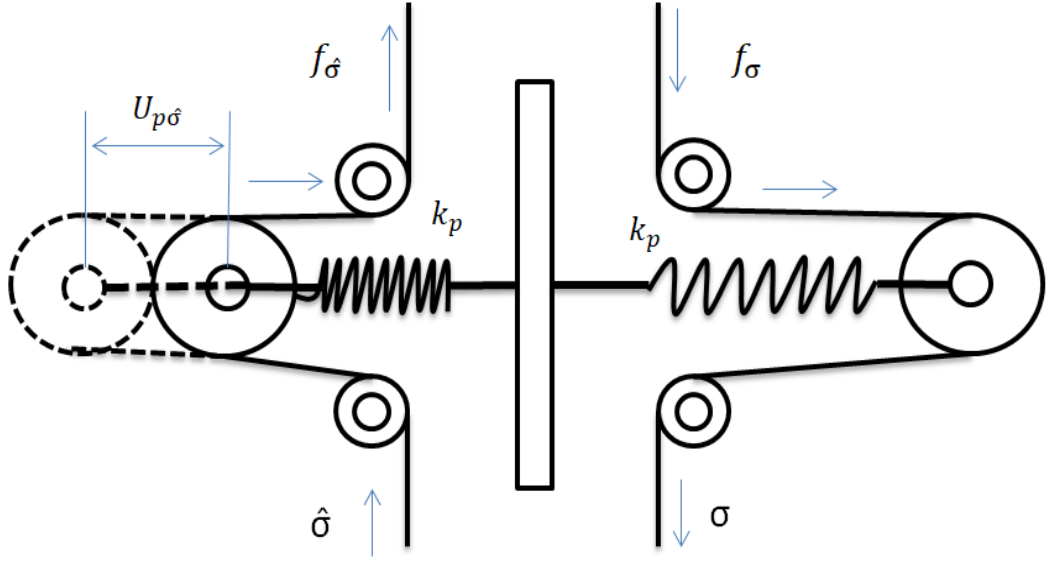
Fig.4-6 Pretension mechanism structure

Let $p_n = (p_{nx} \quad p_{ny} \quad p_{nx})^T$ be the position vector of the end-point and $\phi = (\phi_a \quad \phi_b \quad \phi_c \quad \phi_d)^T$ be rotation angle vector of the 4 motors. Let $T_m = (T_a \quad T_b \quad T_c \quad T_d)^T$ be a torque vector loaded on the motor axes.

The virtual work principle gives an identity;

$$\Delta M g^T \Delta p_n = T_m^T \Delta \phi \qquad (23)$$

where ΔM is a perturbed mass loaded on the end-point and $g = (0 \quad 0 \quad g)^T$ is the gravitation acceleration vector.

If a Jacobian that stipulates a relation between the infinitesimal displacement of the end-point and the infinitesimal rotation of the motors; $J \triangleq \frac{\partial p_n}{\partial \phi} \in \mathfrak{R}^{3 \times 4}$ is available, Eq.(2) becomes,

$$\Delta M g^T J \Delta \phi = T_m^T \Delta \phi \qquad (24)$$

It provides an identity on two vectors in the left and right sides.

$$\Delta M J^T g = T_m \quad \in \mathfrak{R}^4 \qquad (25)$$

Torque loaded about motor axis is related to the wire tension such as,

$$T_\sigma = \frac{\lambda}{2\pi}(f_\sigma - f_{\hat\sigma}), \quad (\sigma = a, b, c, d), (\hat\sigma = \hat a, \hat b, \hat c, \hat d) \qquad (26)$$

Where λ is a lead of the screw (see Fig.2-12).
Substituting (22) into (26), we have

$$T_\sigma = \frac{k_p \lambda}{4\pi}(u_\sigma - u_{\hat\sigma}). \qquad (27)$$

Hence T_m in (24) is obtained by,

$$T_m = \frac{k_p \lambda}{4\pi} \Delta u \qquad (28)$$

where $\Delta u = (u_a - u_{\hat{a}} \quad u_b - u_{\hat{b}} \quad u_c - u_{\hat{c}} \quad u_d - u_{\hat{d}})^T$

Substitution of (28) into (25) gives

$$\Delta M J^T g = \frac{k_p \lambda}{4\pi} \Delta u \tag{29}$$

Since $g = (0 \ 0 \ g)^T$ and $J = \frac{\partial p_n}{\partial \phi} = \left(\frac{\partial p_{nx}}{\partial \phi} \quad \frac{\partial p_{ny}}{\partial \phi} \quad \frac{\partial p_{nz}}{\partial \phi} \right)^T$,

$$J^T g = g \left(\frac{\partial p_{nz}}{\partial \phi} \right)^T = g \left(\frac{\partial p_{nz}}{\partial \phi_a} \quad \frac{\partial p_{nz}}{\partial \phi_b} \quad \frac{\partial p_{nz}}{\partial \phi_c} \quad \frac{\partial p_{nz}}{\partial \phi_d} \right)^T.$$

Hence, (29) is rewritten to,

$$\Delta M g \left(\frac{\partial p_{nz}}{\partial \phi_a} \quad \frac{\partial p_{nz}}{\partial \phi_b} \quad \frac{\partial p_{nz}}{\partial \phi_c} \quad \frac{\partial p_{nz}}{\partial \phi_d} \right)^T = \frac{k_p \lambda}{4\pi} \Delta u \tag{30}$$

which induces,

$$\Delta M g \frac{\partial p_{nz}}{\partial \phi_\sigma} = \frac{k_p \lambda}{4\pi} (u_\sigma - u_{\hat{\sigma}}) = \frac{k_p \lambda}{4\pi} \Delta u_\sigma , \tag{31}$$

$$(\sigma = a, b, c, d)$$

where, $\Delta u_\sigma = u_\sigma - u_{\hat{\sigma}}$. If a perturbed mass ΔM loaded at the end-point is known in advance, (31) will be rewritten to,

$$\frac{\partial p_{nz}}{\partial \phi_\sigma} = \frac{k_p \lambda}{4\pi g} \frac{\Delta u_\sigma}{\Delta M} , \quad (\sigma = a, b, c, d) \tag{32}$$

(32) states that if a small compression/extension Δu_σ of the pretension spring yielded by loading ΔM at the end-point is available, we can estimate the corresponding partial differentiation term of the Jacobian.

Giving a small displacement of the end-point along the z-axis; Δp_{nz} , (32) provides a motor angle to achieve it as,

$$\Delta \phi_\sigma = \left(\frac{\partial p_{nz}}{\partial \phi_\sigma} \right)^{-1} \Delta p_{nz} = \frac{4\pi g}{k_p \lambda} \frac{\Delta M}{\Delta u_\sigma} \Delta p_{nz} , (\sigma = a, b, c, d) \tag{33}$$

Wire-tension control is based on differences in compression length between a pair of pre-tension springs (Eq.26). As the robot takes bending motion, PtM sliders change their positions (Fig.4-7). The linear potentiometers that slide accompanied by the PtM sliders provide compression lengthes of the pretension springs, which are fed back to the controller. This method allows not only maintaining the tension level but also improving robot payload manipulability. The output value of the linear potentiometer ranges from 0 to 1023 (2^{10}), in which within 300 and 800 assures that the wire is not in the state of slacking or high tension (see Fig.4-8).

If a vertical deviation of the end-point Δp_{nz} is obtainable by using a gyro-sensor, e.g., attached at the end-point, Eq. (33) directly determines the rotation angle of motor-σ. However, it is sometimes harmful to put an electronic device at an end-point in some severe environments. Thus, the approach to control the end-point

motion with a simple and empirical C-driving only by using tension information as follows.
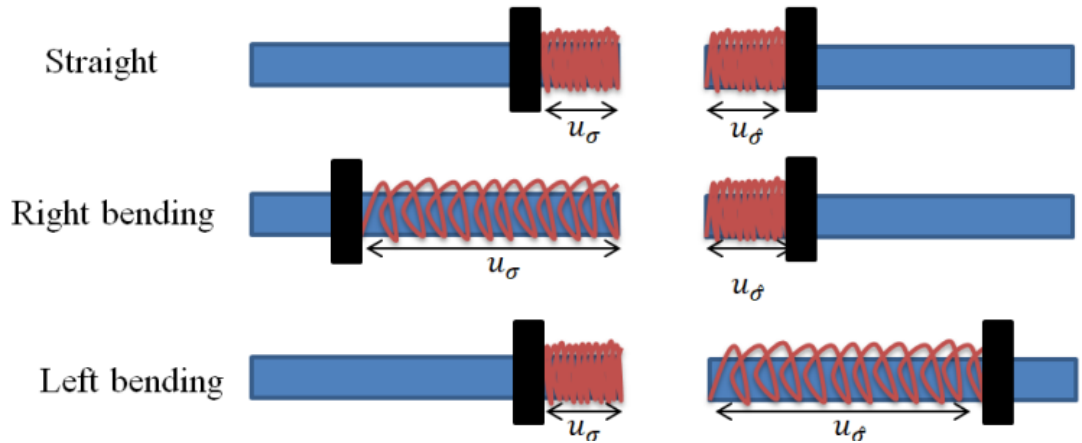

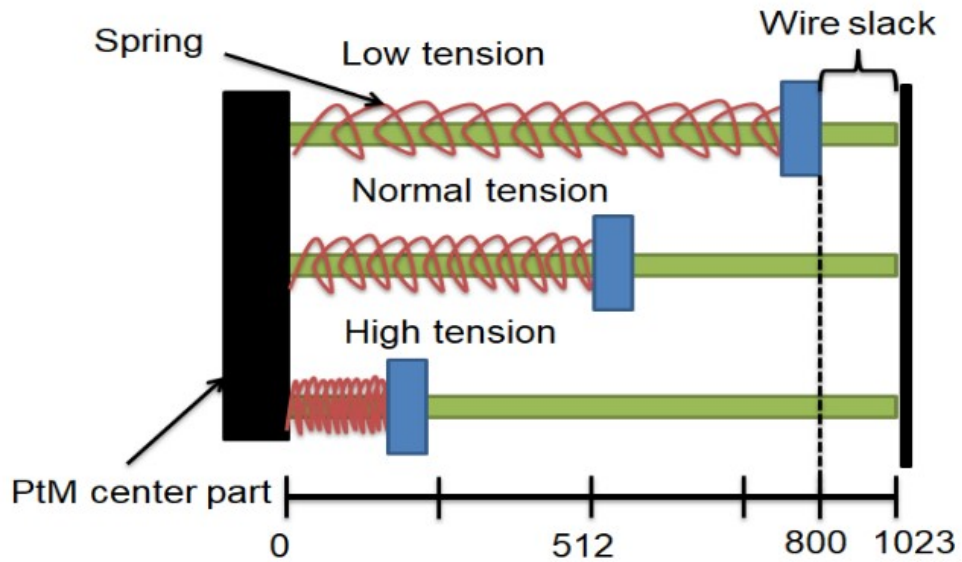Fig.4-7. Pre-tension mechanism slider arrangement

Fig.4-8. Wire-tension level of the PtM device

The control diagram is shown in Fig.4-9. Based on robot actuating design, one motor drives a pair of wires (see Fig.4-10) that go out the actuating unit and enter the PtM device. Inside the PtM, each wire pulls or releases the corresponding spring accompanied by sliding the linear potentiometer of which voltage (tension information) goes to the Arduino. In the case of bending to the left side, the wire-tension of the left side increases as the motor pulls the wire. While the wire-tension of the right side stays almost the current level, because total wire length of the right side becomes elongated with the bending motion, but it is compensated by the motor releasing the wire. As a result, it yields the difference of voltages between the linear potentiometer of the left side and that of the right side.
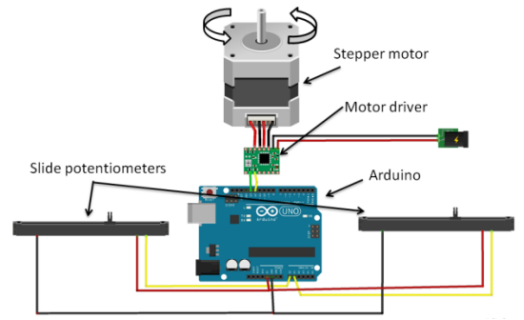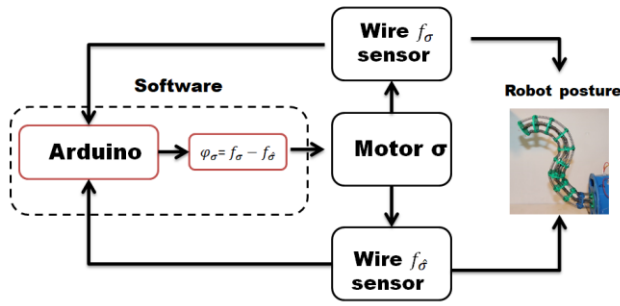
The control block   Single actuating unit schematics
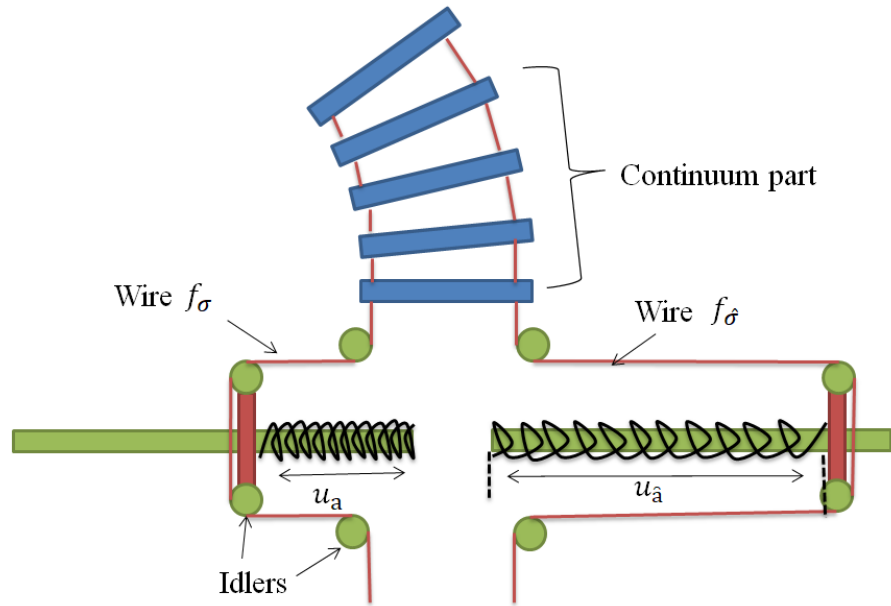Fig.4-9. Control block diagram

Fig.4-10. Linear potentiometers working principle.
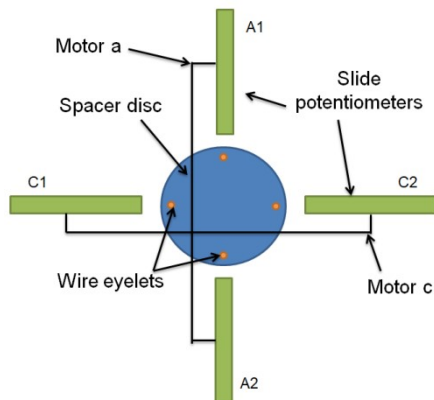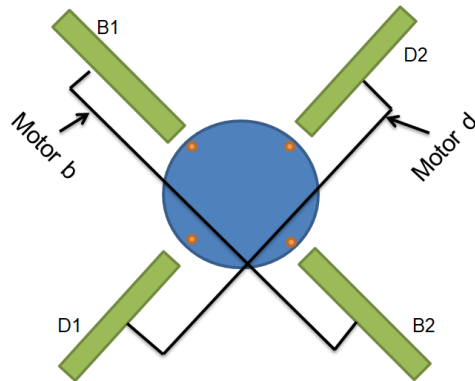
First section   Second section
Fig.4-11. Wire eyelets and linear potentiometer arrangements

Fig.4-11 demonstrates slider arrangements, where it is noted that wires are paired as A1, A2 (wires a, â) and C1, C2 (c, ĉ) for the first section and B1, B2 (b,b̂) and D1, D2 (d,d̂) for the second section. Based on the wire tension level determined by the data obtained by the linear potentiometer, it would use them to predict a vertical deviation of the end-point for further wire-tension compensation.

The proposed pre-tension mechanism provides two types of wire-tension mode; passive mode and active mode. Passive wire-tension compensation is provided by varying the compression length of springs in the PtM when the wire-tension is varied by something external factors, e.g., loading an external weight on the end-point. Active pre-wire-tension compensation is provided by motors to maintain a required wire-tension. In case the complex shape of continuum robot such as 'S' shape, the passive pre-tension mode may not fully handle the wire-tension because of the limited length of slider displacement, which requires the active mode to compensate the wire-tension with the aid of feedback information from linear potentiometers.

To proof, the effectiveness of the pre-tension mechanism, several types of tests were conducted.

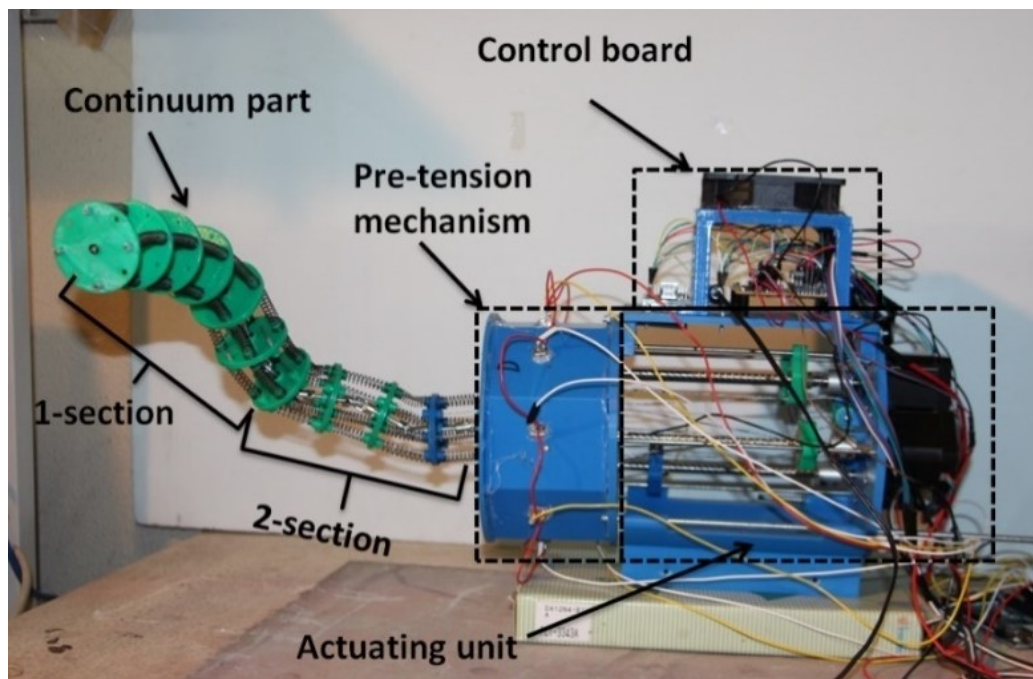## 4.3. Test on basic motions


Fig.4-12. TakoBot experimental setup

The experimental robot setup consists following parts: continuum part, pre-tension mechanism, actuating unit and control board (Fig.4-12). Continuum part consist of two actuated sections, 1st section (distal side) and 2nd section (proximal side). In this experiment the pre-tension mechanism contains linear potentiometer sensors, so in the Fig. 4-12 it is seen the sensors wiring. The robot control box located on the top of the actuating unit, also a cooler had been mounted to prevent electronics overheating.

First, test was the simple bending operation to observe the difference of the resultant shape of the manipulator between the and the prototype with non-sliding discs under the identical motor driving (Fig.4-13). Next, we tested for "S" shaped motion as shown in Fig.4-14. For continuum manipulators, they are frequently required to form an S-shape when in operation. As shown, TakoBot demonstrated more prominent 'S' bending with more small curvature. It is due to the fact that the

sliding disc mechanism allows all joints belonging to the same section to rotate almost evenly.
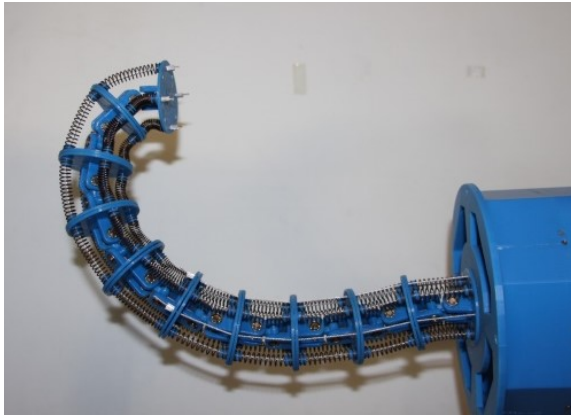
Non-sliding   Sliding
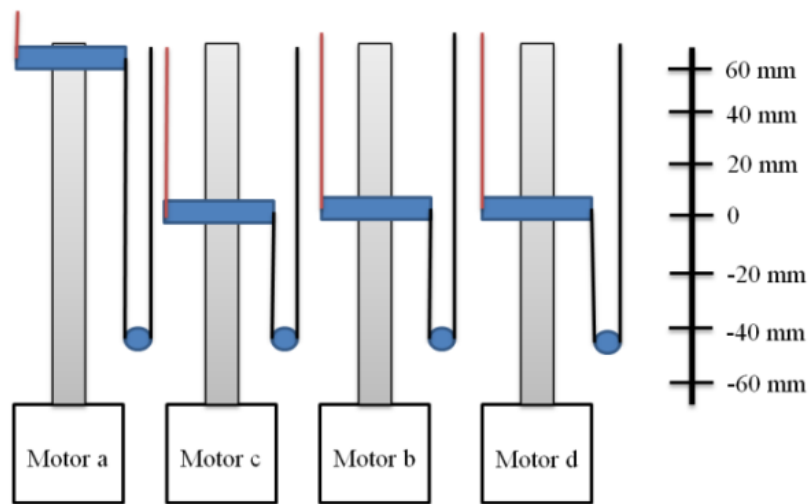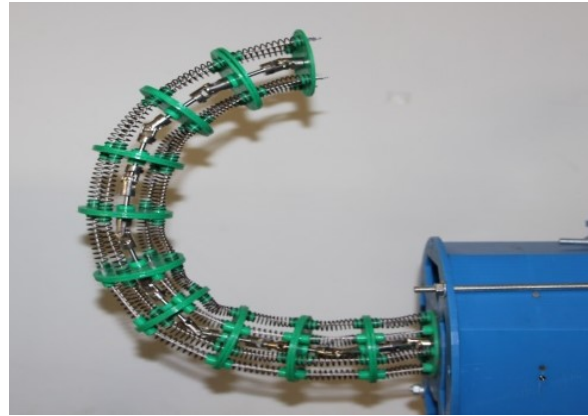
Sliding length of the sliders

Fig.4-13 Bending comparison between prototype model without sliding discs and the TakoBot with sliding discs
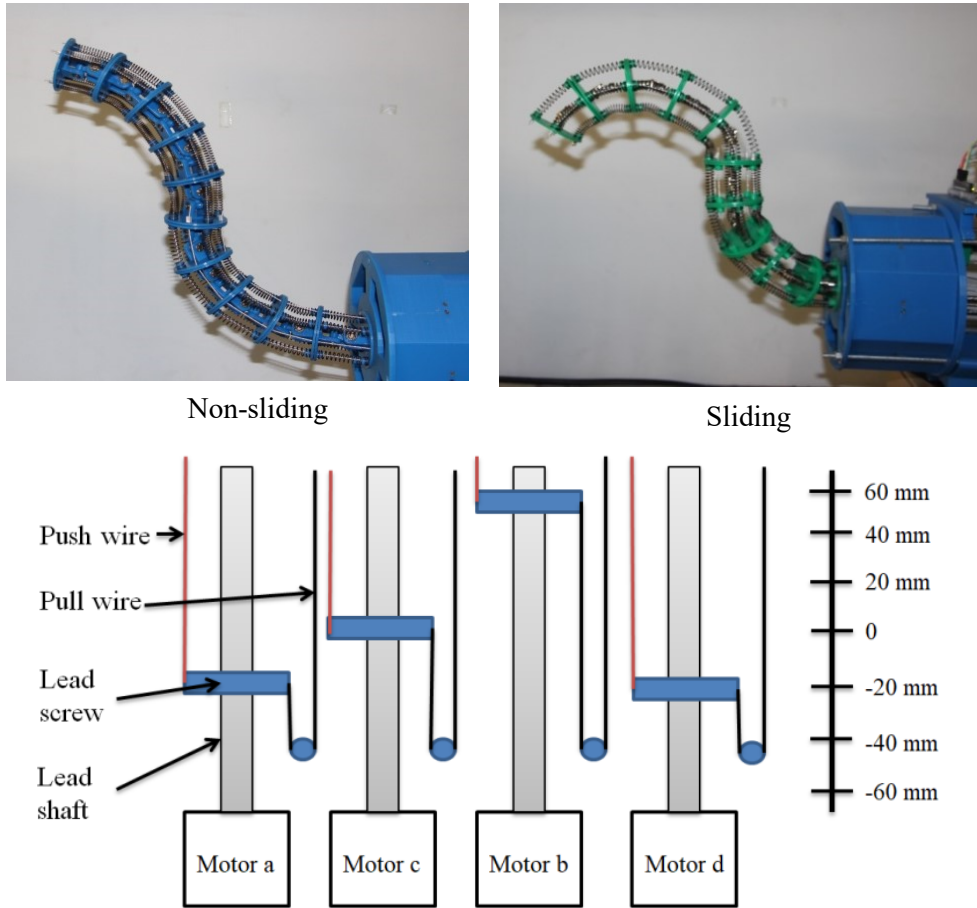
Fig.4-14 "S" shape comparison between prototype model without sliding discs and the TakoBot with sliding discs

Finally, angles between adjacent discs were measured. As shown in Fig.4-15, the disc positions of TakoBot with sliding discs passively change to balance the static force during bending motions. Therefore, it minimized the bending stress along the backbone.

Fig. 4-15. The measurement of disc displacement
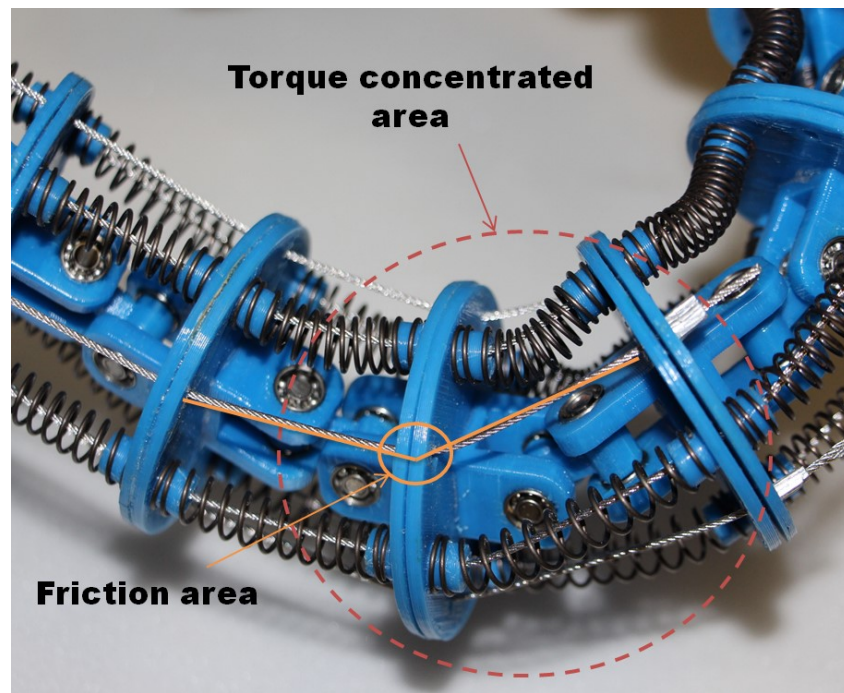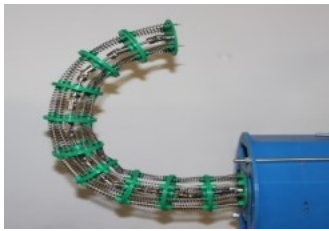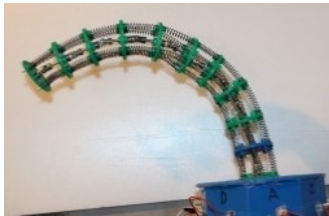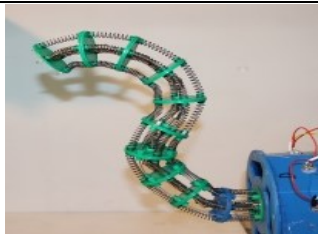
Fig 4-16 Torque concentrated area of non-sliding prototype

In Fig. 4-16 shows that non-sliding backbone prototype cannot spread the bending strain along the continuum backbone to reach pure bending. Therefore in case of bending such design creates an interference between wire and robot parts, which yields an unnecessary torque consumption due to the friction.
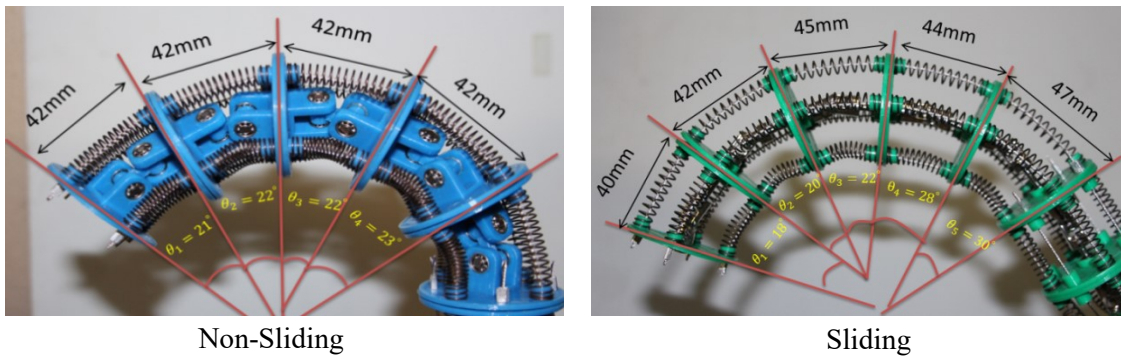
During the conducted experiment it is discovered correlation between wire tension level and the robot output shape. Thus, obtained feedback wire-tension information could be used not only for control, but also could be utilized to predict the robot shape as well. Such method is very useful when the robot is out of user sight.

According to the Fig. 4-7, the wire tension of the robot had been classified into four levels; high tension, normanl tension, low tension and lost tension, such classification is determined based on linear potentiometers value. Thus, all robot shapes are defined with wire-tension combinations (Table 4-2). Proposed hybrid pretension mechanism also has a beneficial features. First of all, sensors are mounted in stationary part of the robot, which means it do not accumulate additional weight to the robot mobile mass. And proposed method with such sensors is cost effective solution. The linear potentiometers are very cheap.

Table 4-2. Robot shape posture control

Basic postures	Combinations
	1st section A1-LT, A2-HT; C1-NT, C2- NT; 2nd section B1-LT, B2-NT; D1-LT, D2-NT
	1st section A1-NT, A2-NT; C1-HT, C2- LT; 2nd section B1-NT, B2-LT; D1-NT, D2-LT
	1st section A1-HT, A2-LT; C1-NT, C2- NT; 2nd section B1-LT, B2-HT; D1-LT, D2-HT
	1st section A1-HT, A2-HT; C1-HT, C2- HT; 2nd section B1-HT, B2-HT; D1-HT, D2-HT
(see Table 4-3 for HT, NT, LT)	

4.4. Test on payload capacity

4.4.1. Lifting up motion

The main purpose of this experiment is to demonstrate the payload capacity of the proposed pre-tension mechanism. In this experiment, the controller orderes a special task to the manipulator, such as, the robot should lift a load mounted on the end-point as high as possible. To do this task, the controller drives motors so as to lift the end-point of the manipulator as high as possible. The experiments were executed by the manipulator with the PtM device and without the PtM devise to evaluate the effectiveness of it (see Fig4-17).
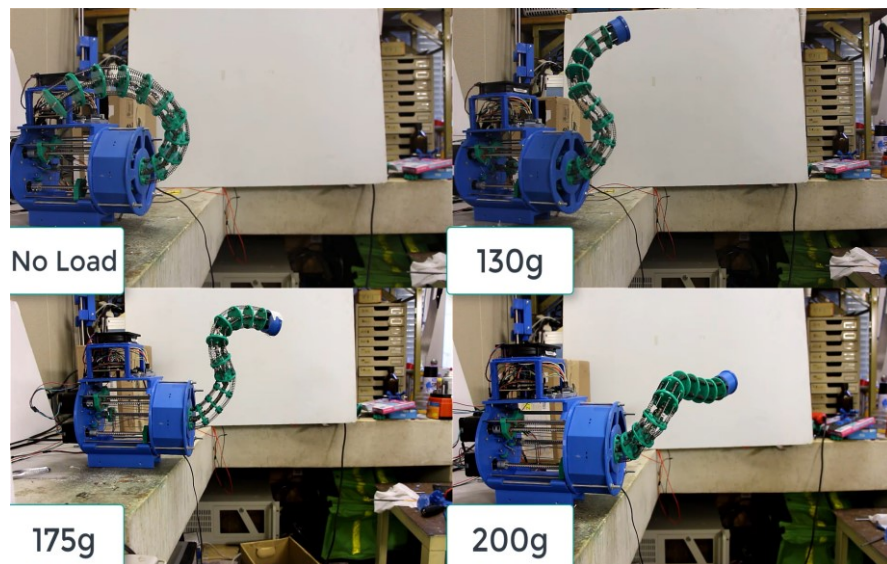
Without PtM device
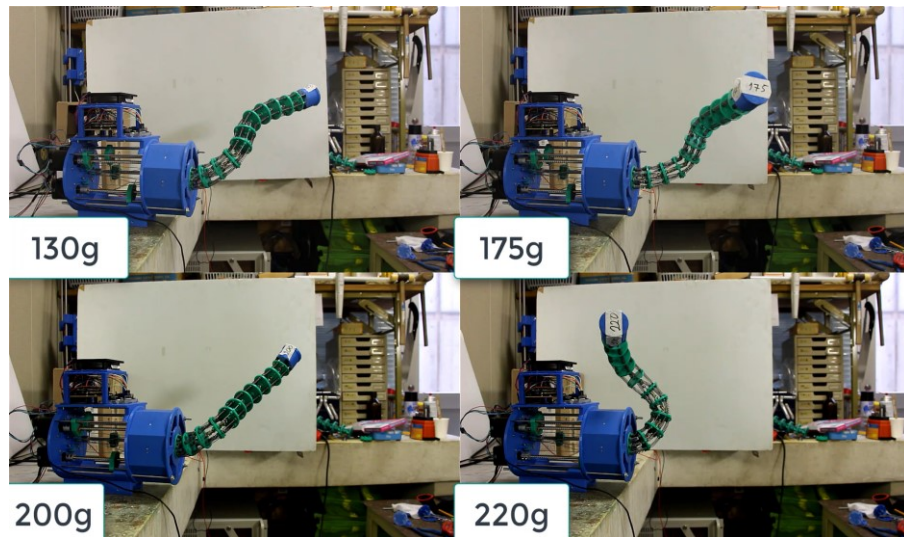
With PtM device
Fig.4-17. Payload test experiment
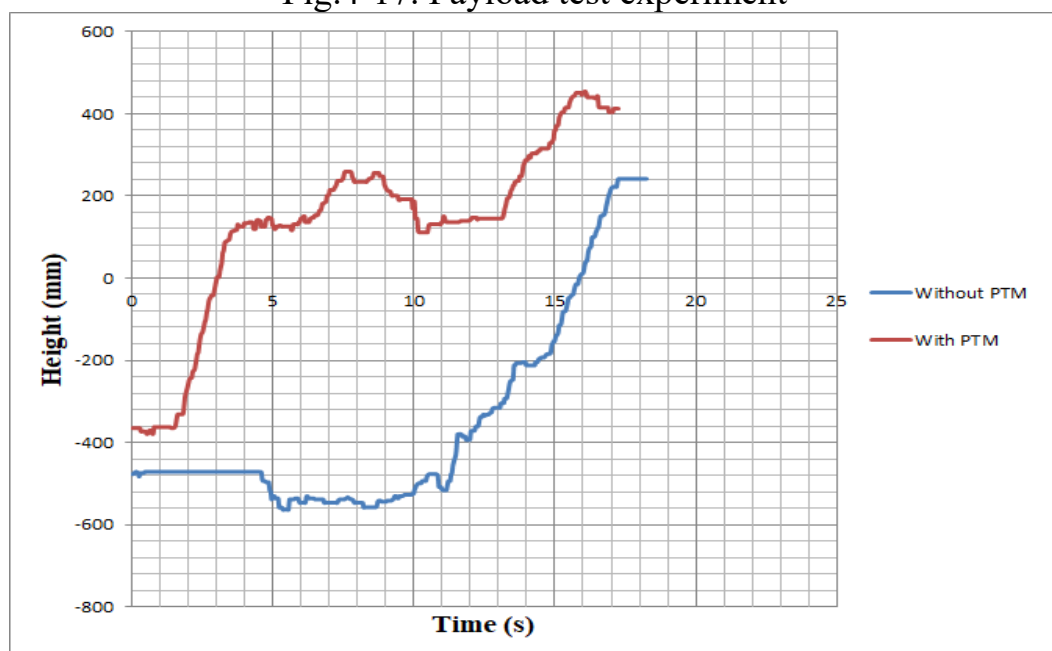
Fig. 4-18. Weight lifting comparison graph. With PtM and without PtM.

To follow the end-effector motion, the traker was used to track the robot path and virtual axes were specified to measure the tracking point locations. According to the obtained results, the pretension mechanism demonstrated better load manipulation and increased robot payload capacity (see Fig.4-18).Takobot with the PtM device was able to manipulate up to 220 g and also demonstrated smooth motion as well. While the one without the PtM device showed a poor payload capacity.

4.4.2 Horizontal moving motion

The purpose of this experiment is to demonstrate the active feedback maintenance of wire-tension. The previous experiment was based on passive wire-tension compensation. To evaluate the active wire-tension compensation, we developed an experimental task. The continuum part should move from left (A-point) to the right (B-point) horizontally, and in this case, motors should compensate the motion of the end-point to move horizontally (see Fig.4-19). To conduct this experiment, we classified the wire-tension levels are classified, so in the case of standby, all wires tension is high tension (HT) (see Table 4-3). Therefore, the vertical sensors (A1A2 see Fig.4-11) should provide high tension levels, while horizontal sensors (C1C2 see Fig.4-11) move from low to high wire-tension level. A motion-tracker that traces the position of points labeled on the video data is used to obtain a path of the end-point on a frontal plane.
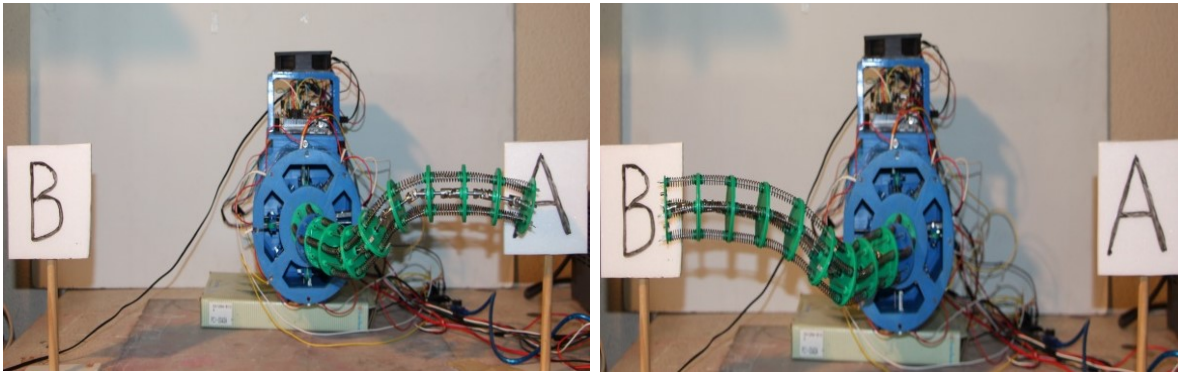
Fig.4-19. Load manipulability experimental setup

Table 4-3. Wire-tension values

Tension level	Data of linear potentiometer (10 bits digital data)
High tension [HT]	$300 < |u_{\Sigma 1} - u_{\Sigma 2}| \leq 600$
Normal-Tension [NT]	$600 \leq |u_{\Sigma 1} - u_{\Sigma 2}| \leq 700$
Low Tension [LT]	$700 \leq |u_{\Sigma 1} - u_{\Sigma 2}| \leq 800$
Tension Loosing	$800 < |u_{\Sigma 1} - u_{\Sigma 2}|$

Here $|u_{\Sigma 1} - u_{\Sigma 2}|$ is an absolute value of the difference between a pair of potentiometers. $u_{\Sigma 1}, u_{\Sigma 2}$ is an individual potentiometer value. As it is shown in the table 4-3, higher value indicates lower wire-tension.

Both cases with C-driving and without C-driving were tested. As an experiment, three loading conditions were approached: no-load, 50g, and 100g. Fig.4-20 demonstrates the differences between using of C-driving and without, which shows a prominent compensatory motion in the case of heavier loads (100g), All of the graphs show some fluctuation, which occurs due to friction between wire and spacer disc eyelets. Furthermore, based on our observation, the C-driving method provides faster speed; wire-tension sensors resultantly contribute a speed-up for stepping motors.

No-load

50 g

100g
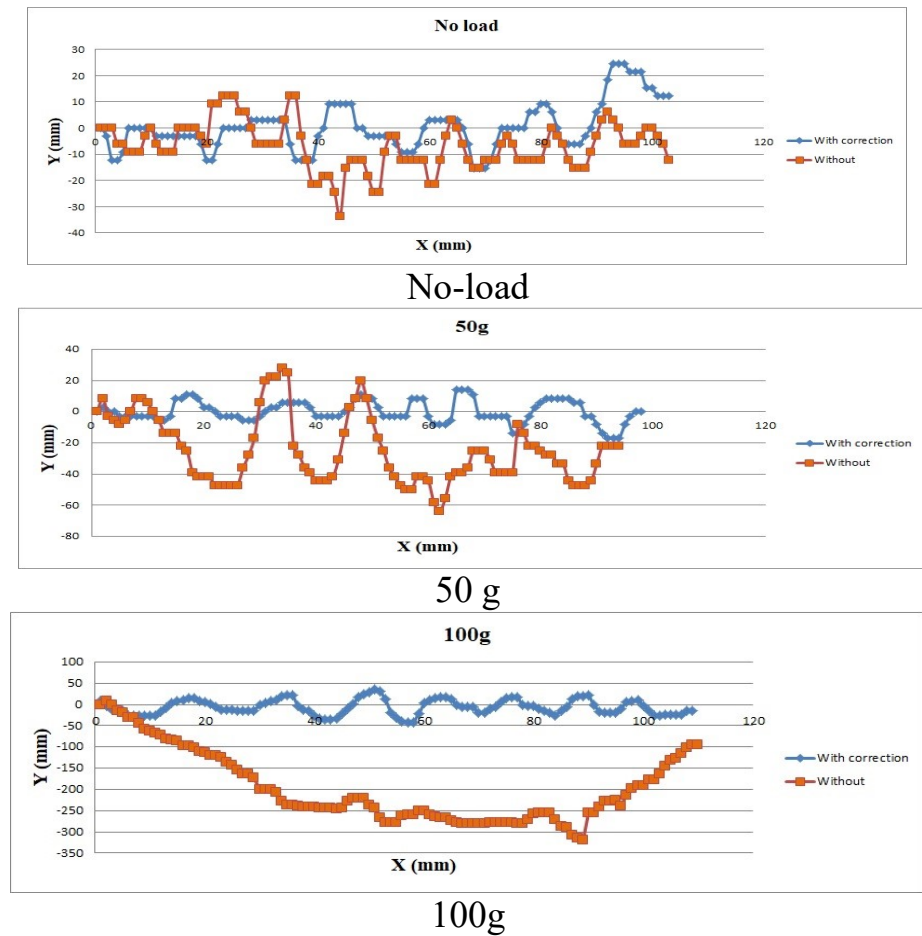
Fig.4-20. Load manipulability graph. The blue curve is with compensation, and the red curve is without compensation.
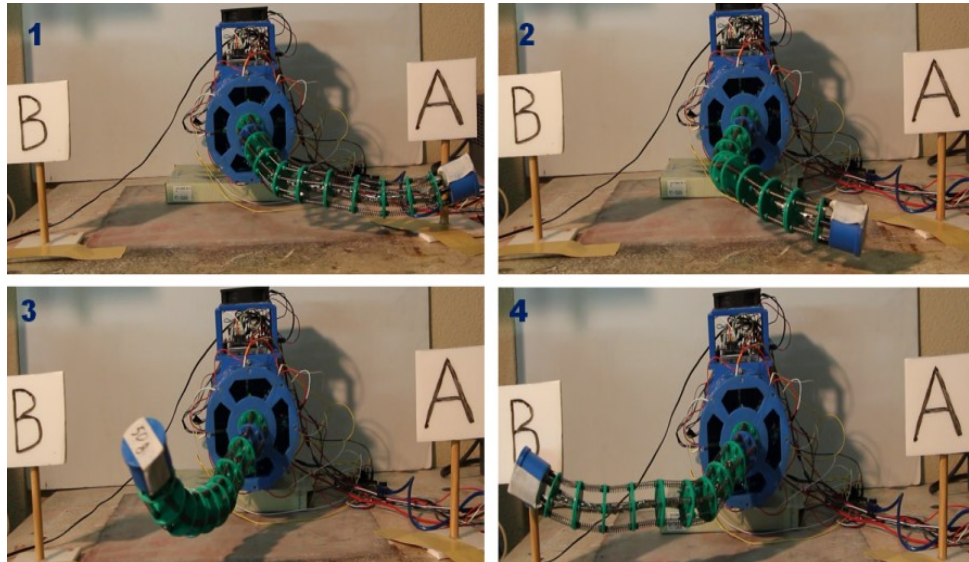
Fig.4-21. 50 g load manipulating experiment

Fig. 4-21 shows the views of the manipulator motion during experiments. The figure describes the four steps of the C-driving experiment from point A to the point B.

4.5. Natural frequency test

In this subsection, the TakoBot natural frequency oscilation is measured experimentally. the end effector tracking system is used to measure the robot oscilation
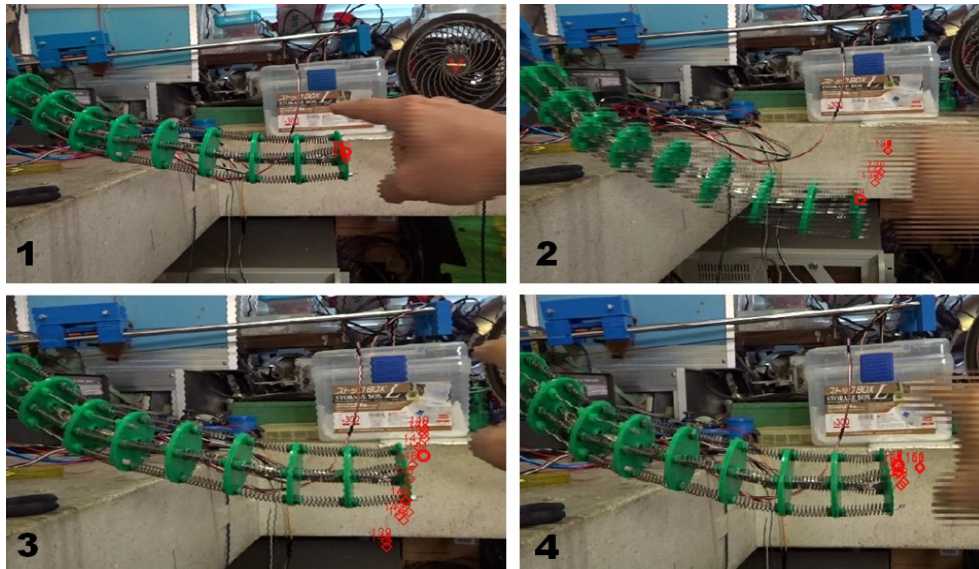
Fig. 4-22. The natural frequency experiment.

Fig. 4-22, demonstrates the steps of TakoBots continuum part oscilation while experiencing with damping force. In the figure, video traker detects the end point and follows by creating a path (see Fig 4-23).
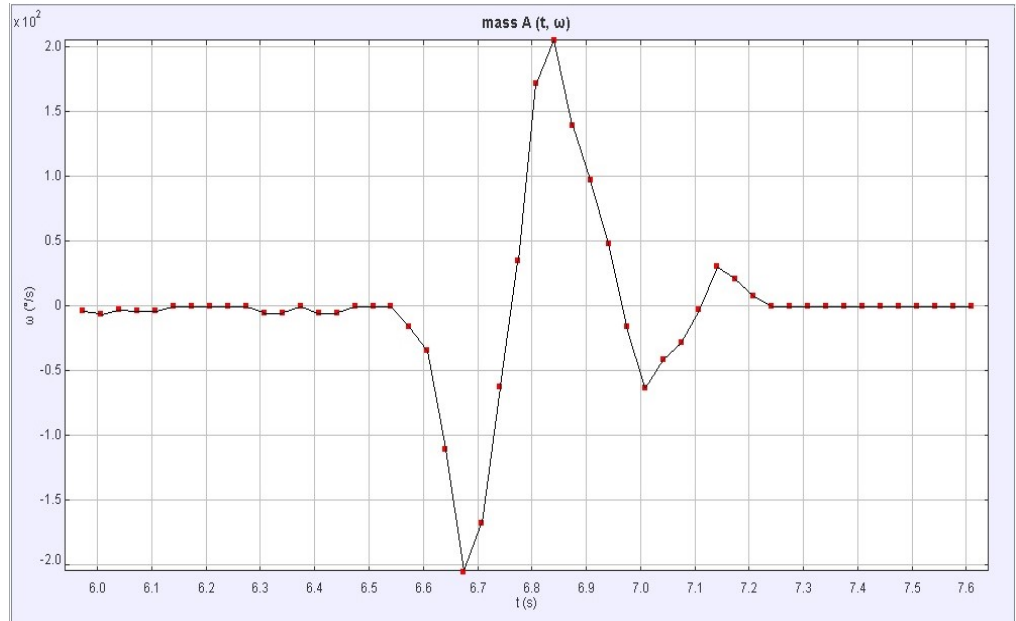
Fig. 4-23. The TakoBot natural frequency graph

According to the obtained result the robot oscilation is about 2Hz

4.6. Conclusive Remarks on Chapter IV

This chapter explained the control architecture of the proposed robot and demonstrated the robot payload test, motion test, natural frequency test. Two types of control had been used in this chapter. Tele-operative control with joystics and compensatory driving with wire-tension feebback control. For the robot compensatory control, the linear potentiometers had been used to obtain a feedback information the actuating continuum part. The linear potentiometers are embedded in the pre-tension mechanism with paired springs to provide tension information to be utilized for compensatory driving. To proof the concept, some experiments had been conducted. Based on the obtained results, the proposed hybrid pretension mechanism with linear potentiometers could be one of the best option in terms of effectiveness and cost efficiency.

Chapter V. ROBOT APPLICATION

5.1. Tomato harvesting application

The proposed wire-driven continuum manipulator has a several potentional ares to be used, such as agricultural sector, rescue operations, repair maintenance, pipeline inspection and in miniaturized size could be used in minimally invasive surgery. Moreover, continuum manipulators are suffering from dynamic affect of gravity. Thus, in space or low gravity areas environment would increase continuum robot capability and dexterity as well.

5.2. Gripper design

The reseach offers a gripper tool with a semi-spherical shape for grasping spherical objects such as a tomato. For detaching tomatoes, cutting blades are added on the edges of the cup. This design allows to separate the tomato in easiest way, and it improves the harvesting time (Fig. 5-1). The gripper cup size is defined by calculating the average size of the cherry tomato. According to our calculations, the diameter of cherry tomatoes is 30-35 mm (Fig.5-2).

a   b

Fig.5-1. a) Gripper CAD design and b) Fabricated prototype
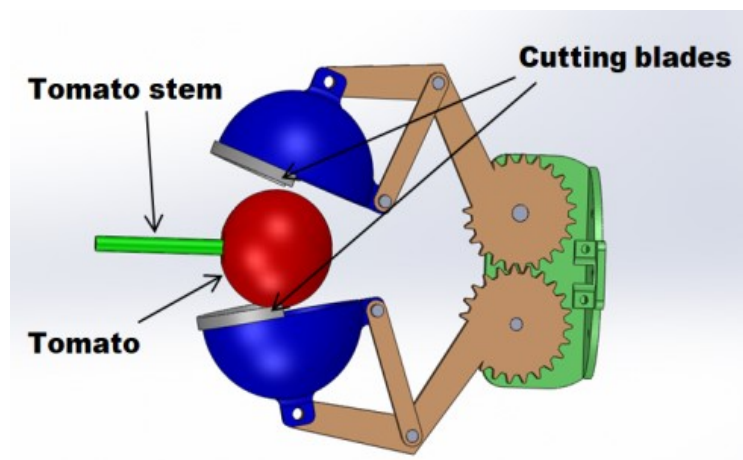
Fig.5-2. Gripper working process

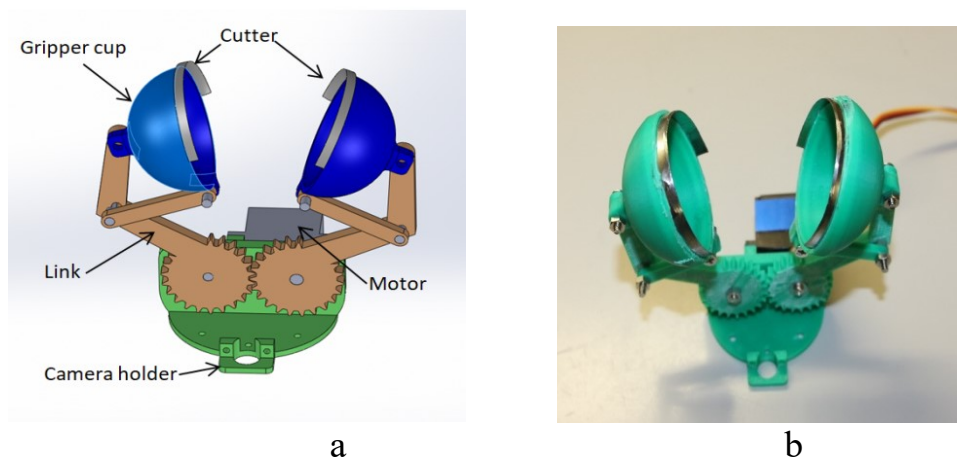Compared with other grippers, this prototype can separate in easiest way and does not require sensors to control it. A lack of electronics allows the robot to work in a wet and highly humid environment. Furthermore, the proposed gripper can cut

the tomato at its sepal, which helps to increase the storage time for harvested tomatoes, while other prototypes leave the sepal on the stem.

5.3. Tomato recognition system

Mature tomato recognition is also a critical part of the robot. This research employs a machine learning to train neural networks to distinguish ripe tomatoes from non-ripe ones and from other similar fruits. As a tomato classifier, YOLO platform had been used. To discriminate tomatoes three main filters had been developed. The first filter detects the shape of the object, the next filter for color or RGB filter, and the third filter is machine learning. This is required because there are many fruits or objects which might be very similar to the tomato, such as an apple or tangerine (Fig.5-3). Moreover, using a classification by camera would make it possible to calculate the distance between the camera and the tomato. For such a technique, a single camera measurement method was used by using the focal length of the camera. The dataset (the tomatoes photos matured and non matured) was collected in Almaty Tomato Greenhouse, in Kazakhstan.
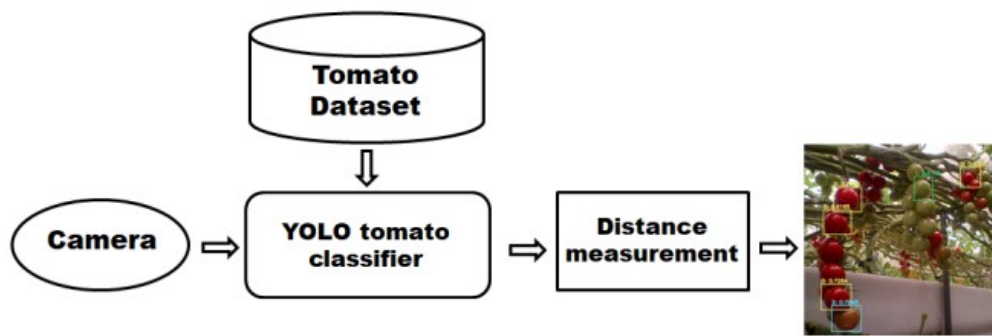
Fig.5-3. Tomato detection architecture

The distance measurement feedback from the camera gives an opportunity to calibrate the gripper tool for perfectly grasping the tomato without any damage (Fig.5-4).
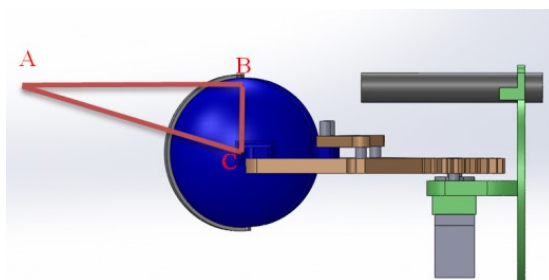
a) CAD View
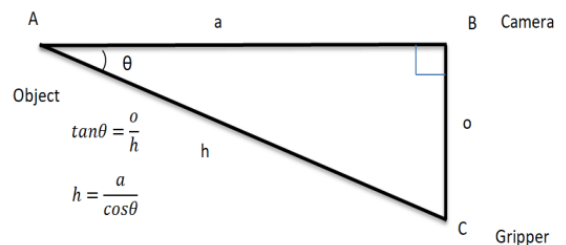
b) geometric formulation

$$tan\theta = \frac{o}{h}$$

$$h = \frac{a}{cos\theta}$$

Fig.5-4. The gripper calibration

Here is o-opposite, h-hypotenuse, and a-adjacent. The opposite distance is fixed, and the adjacent distance comes with the camera. Based on this formulation, it could calibrate the gripper position for accurate grasping.
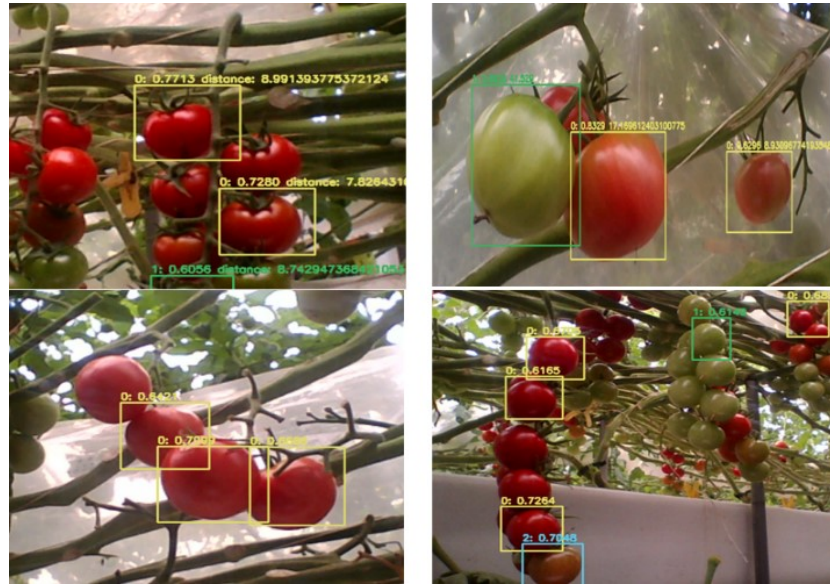
Fig.5-5. Testing of the tomato recognition in a real environment.

In Fig. 5-5, the camera measures the distance and detects mature tomatoes. This experiment had been conducted in Kawasaki tomato greenhouse, Japan. In this research, a borescope camera utilized with a 2-megapixel resolution.

5.4. Control architecture

TakoBot's control architecture consists of two main parts: software (detecting) and hardware (harvesting) (Fig.5-6). The work process starts with the software. Firstly it scans ripe tomatoes. Then, after detecting them, the camera measures distances. Finally, the measured information helps calculate the robot's inverse kinematics to determine motor rotating angles. The calculated inverse kinematics sends the information and coordinates of the tomato to the Arduino board. Thus, the Arduino board sends data to the motors to make the gripper get to the desired position.
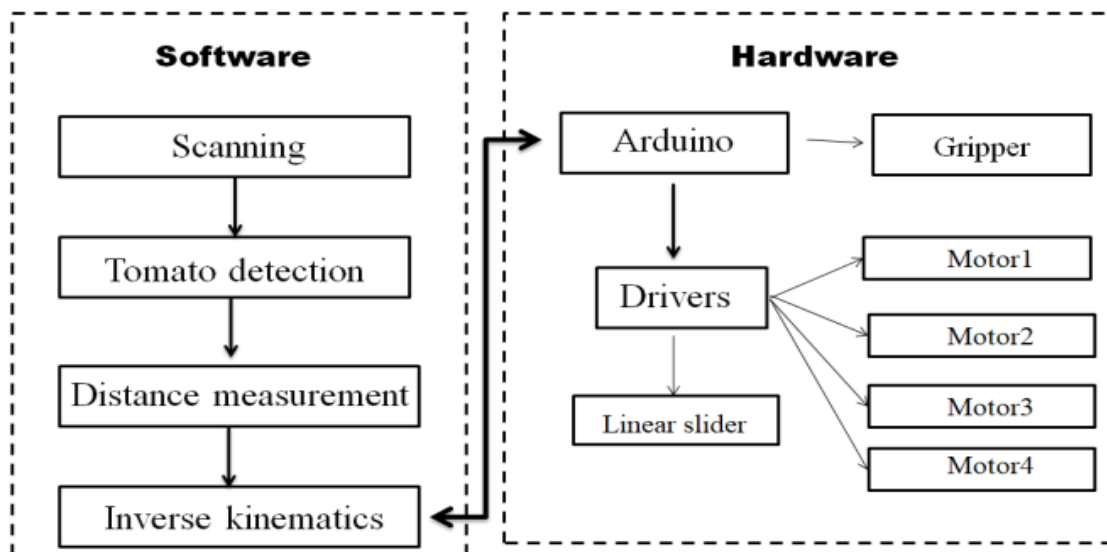
Fig.5-6. TakoBot control architecture

TakoBot has six motors, one micro-servo motor for the gripper tool, and five bipolar stepping motors. Four stepping motors are dedicated to control the manipulator, and one motor is for the linear slider that move the overall TakoBot body. The voltage supply is divided into two level, 12 V for motors and 6V for other electronic components.

For tomato selection, we made an algorithm that measures the priority value P. First of all, the camera detects several tomatoes and makes the decision which tomato should come first and the following picking order. In two-dimensional planes where tomato location is indicated in the frame after it would be measured by horizontal value H and vertical value V, and the sum of two values gives priority value P. Tomato selection priority starts from the lowest value to the highest. The tomato picking diagram is illustrated in Fig. 5-7.

$$P_n = H_n + V_n$$
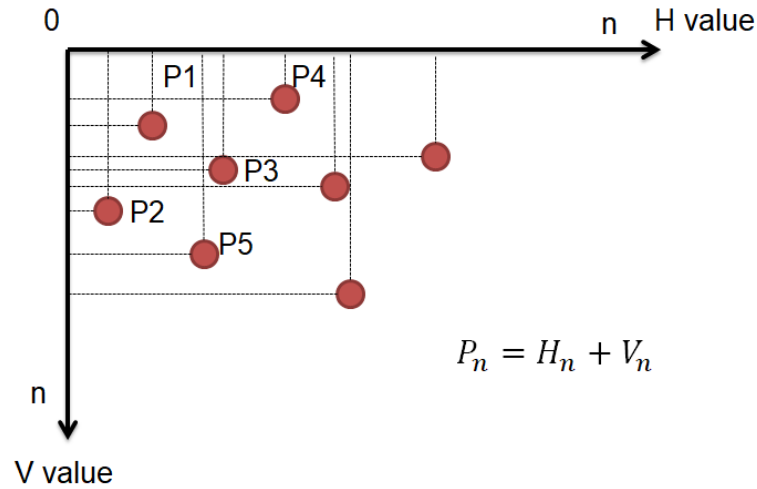
Fig.5-7. Tomato picking priority diagram

5.5. Tomato harvesting experiment

As a controller, an Arduino UNO board and TMC2208 motor drivers for the stepping motors were used. For continuous work, also a cooler was equipped for electronic parts. TakoBot has four motors and one stepping motor for linear motion along with the linear slider, and one micro-servo motor in the end–effector.

For the experiment, by 3d printer cherry tomatoes were fabricated to imitate real cherry tomatoes and hung them in front of the manipulator. The task was to reach and grasp the tomato, detach it from the stem, and put it into the basket. Therefore, during the experiment, the robot manipulability, such as reaching the object from various angles (Fig.5-8) was tested.
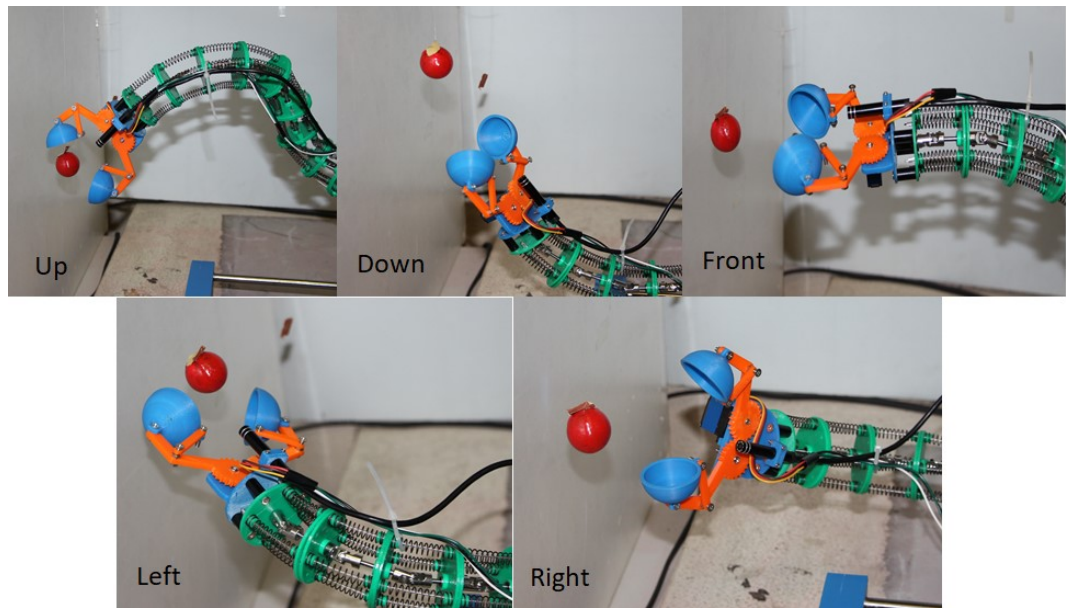
Fig.5-8. TakoBot object reaching angles

According to the conducted experiment observations, TakoBot demonstrated high feasibility in working in a confined workspace as well as reachability. The single-arm was enough to perform the given task.

During the experiment, the harvesting time increased when obstacles existed. In such a case, the continuum part spent more time to fit the newly constrained environment and to reach to the object (Fig.5-9). Furthermore, the tomato grasping process also takes more time. Based on the observed results, almost half of the time of the whole harvesting process was spent to it. However, the success rate of the tomato is pretty high, the manipulator was able to grasp all detected tomatoes, but it spends more time to complete the task.
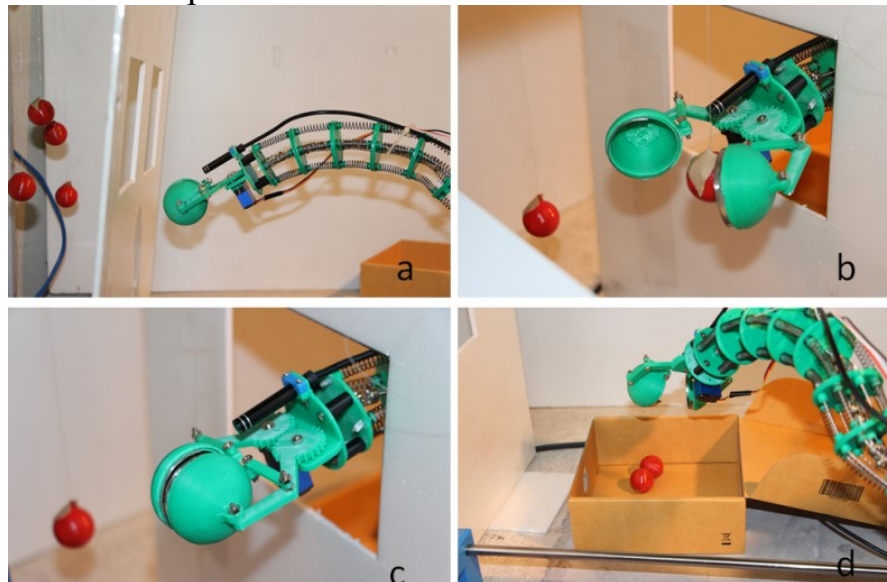
Fig.5-9. Tomato harvesting procedure. a) scanning and reaching for the tomato, b) grasping of the tomato, c) separating of the tomato, d) putting into the basket.

The robot harvesting procedure basically consists of four steps: scanning for the tomato (Fig.5-9); after the detection of the tomato, the robot moves to capture one. The next step after getting close enough is grasping the tomato by the gripper, then

detaching it from the stem, and finally putting it in the basket. The newly developed gripper provides smooth separating of the tomato, which increases the harvesting time and simplifies harvesting tasks. Moreover, TakoBot uses only a single arm for all of these procedures, which makes the robot compact and cost-effective (Fig.5-9).
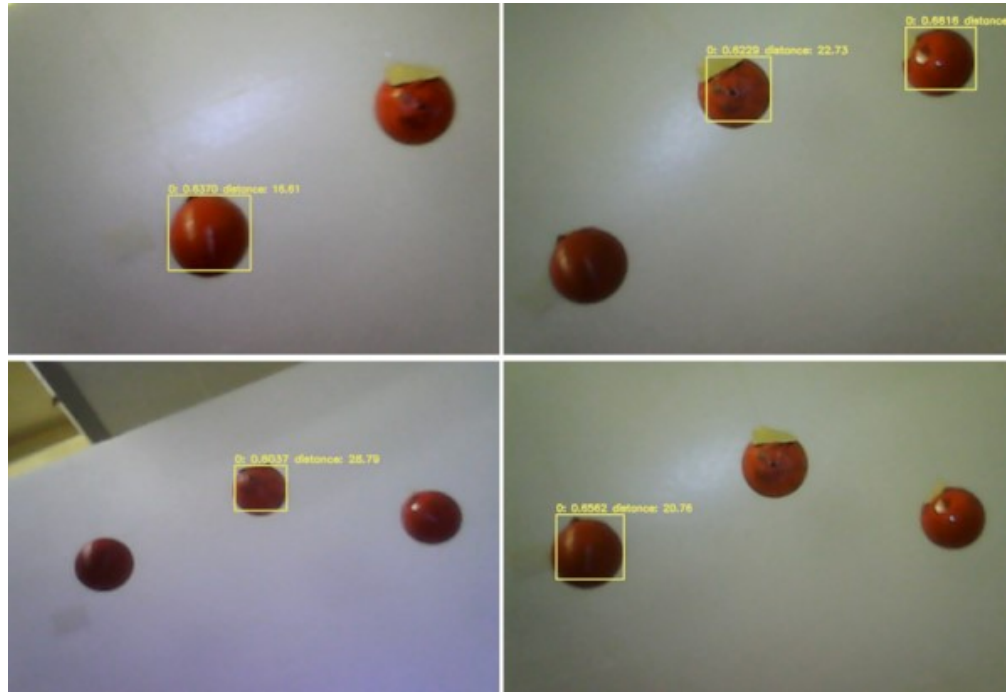
Fig.5-10. Cherry tomato capture and detection during the harvesting process.
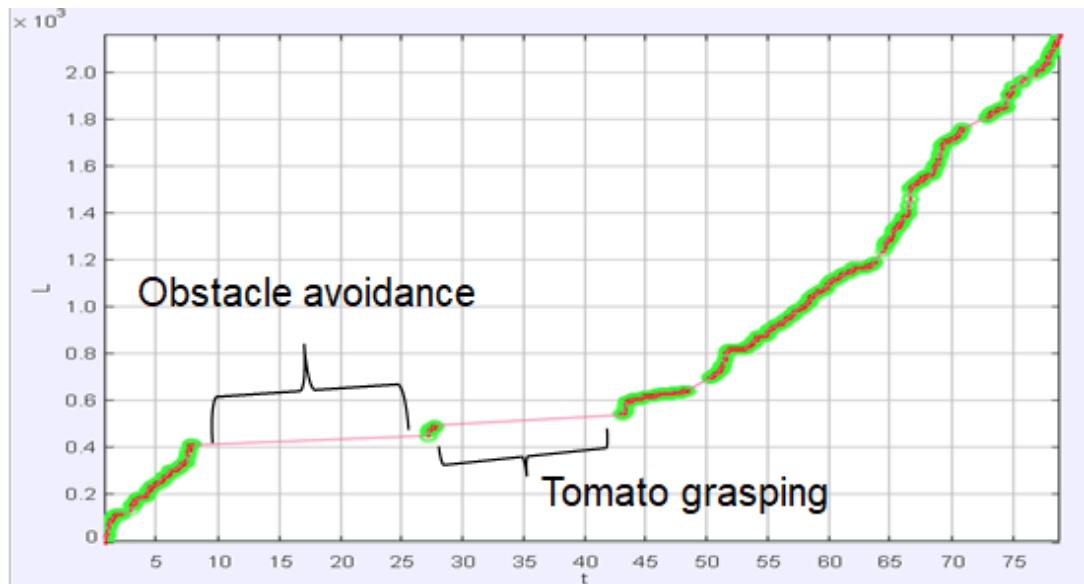
Fig.5-11. Tomato harvesting path length

According to the obtained results, the proposed manipulator is able to manipulate objects up to 200 grams, and during the harvesting process, the robot's slender part reached high stiffness rigidity. Fig. 5-19 shows the captured tomatoes. Such detection would not be possible if the continuum shakes. In terms of speed, the proposed manipulator is slower than commercially available prototypes, but the main

beneficial point of the robot is reachability and tomato selectivity. The conducted experiment demonstrates manipulator ability in working in an extremely confined environment. Moreover, the proposed gripper simplifies the harvesting process by passively cutting the stem.

The application potential of continuum manipulators in the agriculture sector is pretty significant. The proposed manipulator could harvest not only tomatoes and also other vegetables and fruits as well. According to the conducted experiments, the continuum structure represents not only a safety robot arm and also as a more feasible manipulator for the agriculture field.

In the future plan, utilizing of machine learning is planning for manipulator control. According to the obtained data, the manipulator spends more time for obstacle avoidance and tomato grasping, so by using a machine learning tool, the harvesting time and reach the optimal continuum robot shape for fast harvesting can be improved.

Chapter VI. CONCLUSION

This research thesis described the design and kinematic and kinetic formulation of a novel wire-driven discrete continuum robot arm with a passive sliding disc mechanism. Moreover, a new control method and novel wire-tension feedback control were also proposed.

According to the experimental results obtained, the proposed sliding mechanism design demonstrated to provide better dexterity and bending features to a continuum robot in comparison with existing non-sliding prototypes. Moreover, in the case of driving via wires, the sliding backbone prototype showed to reach the desired bending angles with the smaller torque than existing prototypes, which will allow to minimize the motor sizes and optimize overall robot design. Furthermore, a new problem solutions of wire-driven robot arm were discovered as well, for instance, twist motion problem. This is when continuum robot experiences low tension, the robot slender part starts to wrap, and in case of non-sliding prototype it wraps and cannot go back to the intial position. Sliding backbone design became more tolerant to the sliding backbone prototype, because of the redundant rotational feature.

As regards robot control, the control of continuum manipulator is pretty challenging issue because of redundant structure. Such structure requires to drive all motors simultaneously to prevent loosening of the wire and to reach desired bending shape. In this thesis, two control methods had been described: teleoperated control and compensatory driving by employing wire-tension feedback. Teleoperated control mode is the most popular one, because of early application of continuum robots were in non-contact or non-invasive environments such as inspection in nuclear reacter, rescue in destructive fields and minimally invasive surgery with gathering information about patient diagnosis. The compensatory driving mode is an autonomous, it gathers information from linear potentiometers about wire-tension level and based on tension level it would maintain the required wire-tension and provide desired robot shape.

Regarding the robot application, this research showed that the proposed robot had much potential to be utilized in agriculture field such as harvesting of cherry tomatoes. The main reason of using in agriculture field stems from the robot safety feature. The inherited flexible design suits well in confined and fragile environment.

This study offers a new hardware pre-tension mechanism device and a new method to prevent a wire slack in wire-driven continuum manipulators. Proposed device design, mathematic formulation of control strategy, and tension control schematics are was explained and supported by experimental results. According to the obtained results, the proposed pre-tension mechanism demonstrates effectiveness for controlling multi-section continuum manipulators, where the wire-tension problem severely appears compared with single-section manipulators. The compact design and low cost make the device more applicable and affordable. Also, by using the proposed mechanism, the control process and programming code make quite

simple. Furthermore, the proposed mechanism could assist in controlling robot shape by a simple and intuitive way, which will be reinforced by using a machine learning method.

1. The sliding backbone can distribute applied force/torque to all of the segments.

2. In the non-sliding prototype, much of force/torque concentrated on the bending segment that the wires directly connect

In conclusion, the proposed novel continuum robot design could be used in agriculture for inspection purposes in the confined workspace and minimally invasive surgery as well. Moreover, the main advantage of the proposed manipulator is its inherent safety feature to the surrounded environment and the human as well. As future plan, the proposed robot arm is planning to be used in harvesting purpose and utilize the machine learning tool to improve robot kinematics and selectivity. Furthermore, based on conducted experiment on natural frequency of the robot (chapter 4), the proposed robot needs dynamic analysis.

References

1. In, H.K.; Kang, S.K.; Cho, K.J. Capstan Brake: Passive Brake for Tendon-Driven Mechanism. In Proceedings of the 2012 IEEE/RSJ International Conference on Intelligent Robots and Systems, Vilamoura, Portugal, 7–12 October, 2012; pp. 2301–2306.
2. Haiya, K.; Komada, S.; Hirai, J. Tension control for Tendon Mechanisms by Compensation of Nonlinear Spring Characteristic Equation Error. In Proceedings of the 2010 IEEE International Workshop on Advanced Motion Control, Nagaoka, Japan, 21–24 March 2010; pp. 42–47.
3. In, H.; Lee, H.; Jeong, U.; Kang, B.B.; Cho, K.J. Feasibility study of a slack enabling actuator for actuating tendon-driven soft wearable robot without pretension. In Proceedings of the 2015 IEEE International Conference on Robotics and Automation (ICRA), Seattle, WA, USA, 26–30 May 2015; pp. 1229–1234.
4. Tang, N.; Gu, X.; Ren, H. Design, characterization and applications of a novel soft actuator driven by flexible shafts. *Mech. Mach. Theory* **2018**, *122,* 197–218.
5. Webster, R.J.; Jones, B.A. Design and kinematic modelling of constant curvature continuum robots: A review. *Int. J. Robot. Res.* **2010**, *29*, 1661–1683.
6. Yeshmukhametov, A.; Koganezawa, K.; Yamamoto, Y. Design and Kinematics of Cable-Driven Continuum Robot Arm with Universal Joint Backbone. In Proceedings of the IEEE International Conference on Robotics and Biomimetics, Kuala Lumpur, Malaysia, Malaysia, 12–15 December 2018; pp. 2444–2449.
7. Jörg Seume, "Researching the supreme discipline together", *AEROPORT, The aviation magazine of MTU Aero Engines, volume* 01/17, www.aeroreport.du, 2017.
8. Anderson, V.C.; Horn, R.C. Tensor arm manipulator design. *Trans. ASME* **1967**, *67*, 1–12.
9. Lane, D.M.; Davies, J.B.C.; Robinson, G.; D.J. O'Brian. The Amadeus dexterous subsea hand: design modelling, and sensor processing. *IEEE J. Oceanic Eng.* **1999**, *24*, 96–111.
10. Suzumori, K.; Iikira, S.; Tanaka, H. Development of flexible microactuator and its applications to robotic mechanisms. In Proceedings of the IEEE International Conference on Robotics and Automation, Sacramento, CA, USA, 9–11 April 1991; pp. 1622–1627.
11. Wilson, J.F.; Li, D.; Chen, Z.; George, R.T. Flexible robot manipulators and grippers: relatives of elephant trunks and squid tentacles. In *Robots and Biological Systems: Towards a New Bionics?* Springer: Berlin, Heidelberg, Germany, 1993; Volume 102, pp. 474–479.
12. Aoki, T.; Ochiai, A.; Hirose, S. Study on slime robot development of the mobile robot prototype model using bridle bellows. In Proceedings of the IEEE International Conference on Robotics and Automation, New Orleans, LA, USA, 26 April–1 May 2004; pp. 2808–2813.

13. Robinson, G.; Davies, J.B.C. Continuum robots-a state of the art. In Proceedings of the 1999 IEEE International Conference on Robotics and Automation (Cat. No.99CH36288C), Detroit, MI, USA, 10–15 May 1999; pp. 2849–2854.

14. Degani, A.; Choset, H.; Wolf, A.; Zenati, M.A. Highly articulated robotic probe for minimally invasive surgery. In Proceedings of the IEEE International Conference on Robotics and Automation, Orlando, FL, USA, 15–19 May 2006; pp. 4167–4172.

15. Li, Z.; Feeling, J.; Ren, H.; Yu, H. A Novel Tele-Operated Flexible Robot Targeted for Minimally Invasive Robotic Surgery. *Engineering* **2015**, *1,* 73–78.

16. Kang, B.; Koijev, R.; Sinibaldi, E. The First Interlaced Continuum Robot, Devised to Intrinsically Follow the Leader. *PLoS One* **2016**, *11*, e0150278, Doi:10.1371journal.pone.0150278.

17. Ji, D.; Kang, T.H.; Shim, S.; Lee, S.; Hong, J. Wire-driven flexible manipulator with constrained spherical joints for minimally invasive surgery. In *International Journal of Computer Assisted Radiology and Surgery*. Springer: Berlin, Germany, 2019; pp. 1–13.

18. Zhao, B.; Zhang, W.; Zhang, Z.; Zhu, X.; Xu, K. Continuum Manipulator with Redundant Backbones and Constrained Bending Curvature for Continuously Variable Stiffness. In Proceedings of the IEEE International Conference on Intelligent Robots and Systems (IROS), Madrid, Spain, 1–5 October 2018; pp. 7492–7499.

19. Li, Z.; Du, R. Design and analysis of a bio-inspired wire-driven multi-section flexible robot. *Int. J Adv. Robots Syst.* **2013**, *10*, 1–9.

20. D.Caleb Rucker, Robert J Webster III, "Statics and Dynamics of Continuum Robots With General Tendon Routing and External Loading", *IEEE TRANSACTIONS ON* ROBOTICS, vol.27.NO.6.December 2011

21. Guochen Niu, Li Wang and Guanghua Zong, Attitude control based on fuzzy logic for continuum aircraft fuel tank inspection robot, 29 (2015)

22. Zheng li, Liao Wu, Hongliang Ren, Haoyong Yu, Kinematic comparison of surgical tendon-driven manipulators and concentric tube manipulators, *Machine and Mechanism,* 148-165 pp, (2017)

23. Kun Cao, et.al. Workspace Analysis of tendon –driven Continuum Robots Based on *Mechanical Interference Identification, Journal of Mechanical Design*, 2017.

24. Anderson, V.C.; Horn, R.C. Tensor arm manipulator design. *Trans. ASME* **1967**, *67*, 1–12.

25. Xin Dong, and et.al, A Novel Continuum Robot Using Twin-Pivot Compliant Joints: Design, Modelling, and Validation., *Journal of Mechanisms* and Robotics, 2016.

26. Rob Buckingham, Andrew Graham, (2012) "Nuclear snake-arm robots", Industrial Robot: *An International Journal* ,Vol. 39 Issue:1 pp. 6-11, https://doi.org/10.1108/01439911211192448

27. Michael W. Hannan and Ian D. Walker, Kinematics and the Implementation of an Elephant's Trunk Manipulator and Other Continuum Style Robots, *Journal of Field Robotics,* volume 20, Issue 2, pp 45-63, https://doi.org/10.1002/rob.10070

28. M.D. Grissom, I.D Walker, Design and experimental testing of the OctArm soft robot manipulator, *Proc. Of SPIE*, 2006.

29. W. McMahan, I.D. Walker field Trials and Testing of the OctArm Continuum Manipulators, pp. 2336-2341, Proceedings of 2006 IEEE International Conference on Robotics and Automation, Orlando, Florida, 2006.

30. P.E. Dupont, J. Lock, B. Itkowitz and E. Butler, Design and Control of Concentric-Tube robots, Vol.26, No.2, pp. 209-225, *IEEE Trans. Robotics.,* 2010.

31. P. Sears and P.E. Dupont, Inverse Kinematics of Concentric Tube Steerable needles, pp. 1887-1892, IEEE International Conference on Robotics and Automation, Roma, Italy, April 2007.

32. L.A. Lyons, R. J. Webster III and R. Alterovitz, Motion planning for active Cannulas, pp.801-806, IEEE/RSJ International Conference on Intelligent Robots and Systems (IROS), Oct. 2009.

33. D.C. Rucker, B.A. Jones and R.J. Webster III, A geometrically Exact Model for Externally Loaded Concentric-Tube Continuum Robots, Vol.26, №5, *IEEE Transactions on Robotics*, Oct2010.

34. R.H. Sturges, S. Laowattana, A flexible tendon controlled device for endoscopy, pp 2582-2591, Proceedings of the 1991 IEEE International Conference and Automation, Sacramento, California, April, 1991.

35. Bo Ouyang, Yunhui Liu and Dong Sun Design Shape Control of a Three-section Continuum Robot, pp. 1151-1156, Proceeding of the 2016 IEEE International Conference on Advanced Intelligent Mechatronics, Banff, Alberta, Canada, July 12-15, 2016

36. B.A. Jones and I.D. Walker, Kinematics for multisection continuum robots, *IEEE TransRobotics*, vol 43-55,2006

37. B.A. Jones and I.D. Walker, *Practical kinematics for real-time implementation continuum robots*, *IEEE TransRobotics*, vol 22, pp 1087-1099, 2006

38. J. Burgner, D.C. Rucker, H.B. Gilbert, P.J. Swaney, P.T. Russel, K.D. Weaver at.all, A telerobotic system for transnasal surgery, *IEEE/ASME Trans. Mechatronics*, vol 19, 996-1006, 2014

39. D. Trivedi, A. Lotfi, and C.D. Rahn, Geometrically exact module for soft robotic manipulators, *IEEE TransRobot*, vol24, pp 773-780, 2008.

40. D.C. Rucker, B.A. Jones, R.S. Webster, A geometrically exact model for externally loaded concentric-tube continuum robots, IEEE TransRobot, vol 26, pp 769-780, 2010.

41. D.B. Camarillo, C.F. Milne, C.R. Carlson, M.R. Zinn, and J.K. Salisbury, Mechanics modelling of tendon –driven continuum manipulators, IEEE TransRobot, vol 24, pp 1262-1273, 2008.

42. A. Yeshmukhametov, Z. Buribayev, Y. Amirgaliyev and R. Ramakrishanan. "Modeling and Validation of New Continuum Robot Backbone Design With

Variable Stiffness Inspired from Elephant Trunk" IOP conference series on material science and engineering, ICMMR 2018, Tokyo, July, 2018.

43. A. Yeshmukhametov, K. Koganezawa and Y. Yamamoto, "A Novel Discrete Wire-Driven Continuum Robot Arm with Passive Sliding Disc: Design, Kinematics and Passive Tension Control", Robotics Journal, MDPI, July 2019

44. Trivedi, D., Rahn, C. D., Kier, W.M., and Walker, I. D., 2008, "Soft Robotics: Biological Inspiration, State of the Art, Future Research," Appl. Bionics Biomech., 5(2), pp, 99-117.

45. Axinte, D. et al., " MiRoR-Miniturazed Robotic Systems for Holistic In-Situ Repair and Maintenance Works in Restrained and Hazardous Environment" IEEE-ASME Trans. Mech., 23(2), pp. 978-981.

46. Burgner-Kahrs, J., Rucker, D C., and Choset, H., 2015, " Continuum Robots for Medical Applications: A Survey," IEEE Trans. Robot., 3196), pp. 1261-1280.

47. Dong, X., et al., "Development of a Slender Continuum Robotics System for On-Wing Inspection/Repair of Gas Turbine Engines," Robot. Cim-Int. Manufac., 44(C), pp.218-229.

48. Gravagne, I., et al., "Large Deflection Dynamics and Control for Planar Continuum Robots," IEEE-ASME Trans. Mech., 8(2),pp 299-307.

49. Gravagne, I., and Walker, I. D., 2002, "Manipulability, Force and Compliance Analysis for Planar Continuum Manipulators," IEEE Trans. Robot., 30(4), pp. 880-889.

50. Buckingham, R., 2002, "Snake Arm Robots," Ind.Robt., 29(3) pp. 242-245.

51. Mahl, T., Hildebrant, A., and Sawodny, O., 2014, "A Variable Curvature Continuum Kinematics for Kinematic Control of the Bionic Handling Assistant," IEEE Trans. Robot., 30(4), pp. 935-949.

52. Y. Asano et al., " A sensor-driver Integrated Muscle Module with High-tension Measurability and Flexibility for Tendon-driven Robots," IEEE/RSJ International Conference on Intelligent Robots and Systems (IROS), Congress Center Hamburg, Oct. 2015, Germany.

53. Mu-Tan Yan, Pin-Hsum Huang, "Accuracy improvement of wire-EDM by real-time wire tension control," Machine Tools & Manufacture, 44 (2004) 807-814.

54. J.Back et al., "Tension Sensing for a Linear Actuated Catheter Robot," Springer International Publishing Switzerland 2015, ICIRA 2015, pp. 472-482.

55. Back J, Linderoth L, Rhode K, and Liu H, "Model-free position Control for Cardiac Ablation Catheter Steering Using Electromagnetic Position Tracking and Tension Feedback," Front.Robot.AI 4:May 2017.

56. Q. Li, J. Bai, Y. Fan, Z. Zhang, " Study of wire tension control system based on closed loop PID control in HS-WEDM. Int. J.Adv.Manuf. Technol (2016)82:1089-1097.

57. J. Kwak, W. Choi and S. Oh, "Modal Force and Torque Control with Wire-Tension Control Using Series Elastic Actuator for Weight Support System", IECON 2017 - 43rd Annual Conference of the IEEE Industrial Electronics Society, October 2017.

58. B.Mitsantisuk, K. Ohishi and S. Katsura. "Control of Interaction Force of Twin Direct-Drive Motor System Using Variable Wire Rope Tension With Multisensor Integration", IEEE Trans. Industrial Electronics, vol 59, no 1. January 2012.

59. S.J.Phee, A.P. Kencana, V.A. Huynh, Z.L. Sun, S.C.Low, K Yang. D Lomanto, K.Y. Ho, "Design of a master and slave transluminal endoscopic robot for natural orifice transluminal endoscopic surgery", Journal of Mechanical Engineering Science, vols(203-210), July 2010.

60. HyunKi In, SungKu Kang, and Kyu-Jin Cho, "Capstan Brake: Passive Brake for Tendon-Driven Mechanism", International Conference on Intelligent Robots and Systems. October, 2012, Vilamoura, Alvagre, Portugal.

61. A.Yeshmukhametov, K. Koganezawa, A. Seidakhmet and Y. Yamamoto. " A Novel Passive Pretension Mechanism for Wire-Driven Discrete Continuum Manipulators", IEEE International Symposium on System Integration (SII2020), January, Honolulu, USA

62. The World Bank , Global consumption database for 2019, fresh or chilled vegetables section, 2019.

63. Zhao Y., Gong L., Liu C., Huang Y., "Dual-arm Robot Design and Testing for Harvesting Tomato in Greenhouse", International Federation of Automatic Control, Elsevier, 2016.

64. Ling X., Zhao Y., Gong L., Liu C., and Wang T., "Dual-arm cooperation and implementing for robotic harvesting tomato using binocular vision", Robotics and Autonomous Systems, Elsevier, 2019.

65. Feng Q., Wang X., Wang G., Li Z. " Design and Test of Tomatoes Harvesting Robot", Proceedings of the 2015 IEEE International Conference on Information and Automation. Liajiang, China, August, 2015.

66. Takaaki Tokunawa, Koichi Oka and Akinori Harada, " 1 segment continuum Manipulator for Automatic Harvesting Robot: prototype and Modeling", Proceedings of 2017 IEEE International Conference on Mechatronics and Automation, August, Japan, 2017.

67. E.J. van Henten, J. Hemming, B. Van Tuiji, J. Kornet, J. Meuleman, J. Bontsema, and E. Van Os, "An autonomous robot for harvesting cucumbers in greenhouses", Autonomous Robots, vol. 13, no. 3,pp. 241-258, 2002

68. S. Hayashi, K. Shigematsu. S. Yamamoto, K. Kobayashi, Y. Kohno, J. Kamata, and M. Kurita, " Evaluation of a strawberry-harvesting robot in a field test", Biosystems engineering, vol. 105, no. 2, pp. 160-171, 2010.

69. Hiroaki Y, Kotaro N, Takaomi H, and Masayuki I, " Development of An Autonomous Tomato Harvesting Robot with Rotational Plucking Gripper". 2016 IEEE/RSJ International Conference on Intelligent Robots and Systems (IROS), Daejeon Convention Center, October, 2016, Korea

70. Root AI company, "Intro Virgo", https://root-ai.com/#intro, 2019.

71. Panasonic company, "Introducing AI-equipped Tomato Harvesting Robots to Farms May Help to Create Jobs", https://news.panasonic.com/global/stories/2018/57801.html, 2018.

72. Yuanshen Z, Liang G, Yixiang H, Chengliang L, Robust Tomato Recognition

for Robotic Harvesting Using Feature Images Fusion, Sensors journal, mpdi, 2016, 16, 173.

73. Takeshi Yoshida, Takanori Fukao and Takaomi Hasegawa, "A Tomato Recognition Mehod for Harvesting with Robots Using Point Clouds" Proceedings of the 2019 IEEE/ SICE International Symposium on System Integration , Paris, France, January, 2019.

74. Takeshi Yoshida, Takanori Fukao and Takaomi Hasegawa, "Fast Detection of Tomato Peduncle Using Point Cloud with a Harvesting Robot" Journal of Robotics and Mechatronics Vol. 30 No.2, 2018.

75. Xiangyu Chen et all., " Reasoning –Based Vision Recognition for Agricultural Humanoid Robot toward Tomato Harvesting", 2015 IEEE/ RSJ International Conference on Intelligent Robots and Systems (IROS), September, Hamburg, Germany.

76. Li Biqing, Ling Yongfa, Zhang Hongyan, Zheng Shiyong, " The design and Realization of Cherry Tomato Harvesting Robot based on IOT" iJOE Vol. 12, Issue 12, 2016.

77. Yasukawa S., Li B., Sonoda t., Ishii K., " Development of a Tomato Harvesting Robot", 2017 International Conference on Artificial Life and Robotics (ICAROB 2017), January, Miyazaki, Japan.

78. Jorge I, Arande-Sanchez, Arturo Baltazar, Gustavo G.A., "Implementation of a Bayessian classifier using repeated measurements for discrimination of a tomato fruit ripening stages". Biosystems Engineering, Elsevier 2008.

79. Baohua Z., Jun Z., Yimeng M., Na Z., Baoxing G., Zhengong Y., Sunusi I.I., " Comparative study of mechanical damage caused by a two-finger tomato gripper with different robotic grasping patters for harvesting robots", Biosystems Engineering , Elsevier 2018.

80. Li Zhang et all. " Deep Learning Based Improved Classification System for Designing Tomato Harvesting Robot", IEEE Access , Multidisciplinary, 2018.

81. Jingui W., Baohua Z., Jun Z., Yinjun X., Baoxing G., And Xialong Y., "Automatic Recognition of Ripening Tomatoes by Combining Multi-Feature Fusion with Bi-Layer Classification Strategy for Harvesting Robots", Sensors, MDPI, 2019.

82. Ooi, Peng Toon et al., "Autonomous Tomato Harvesting Robotic System in Greenhouses: Deep Learning Classification", Journal of Intelligent Manufacturing & Mechatronics, Vol. 01, issue 01, 80-86, 2019.

83. Zhiguo L., Fengli M., Zhibo Y., Pengpeng G., Shanju Y., "Factors affecting human hand grasp type in tomato fruit-picking: A statistical investigation for ergonomic development of harvesting robot", Computers and Electronics in Agriculture, Elsevier 2019.